REPORT CDOT-2021-08 FEBRUARY 2021

IN-SITU MONITORING OF INFILTRATION-INDUCED INSTABILITY OF I-70 EMBANKMENT WEST OF THE EISENHOWER-JOHNSON MEMORIAL TUNNELS, PHASE III

APPLIED RESEARCH &
INNOVATION BRANCH

Alexandra Wayllace, CSM
Ning Lu, CSM
Benjamin Mirus, USGS

COLORADO
Department of Transportation

Technical Report Documentation Page

1. Report No.	2. Government Accession No.	3. Recipient's Catalog No.
CDOT 2021-08		

4. Title and Subtitle	5. Report Date
IN-SITU MONITORING OF INFILTRATION-INDUCED INSTABILITY OF I-70 EMBANKMENT WEST OF THE EISENHOWER-JOHNSON MEMORIAL TUNNELS, PHASE III	February 2021
	6. Performing Organization Code

7. Author(s)	8. Performing Organization Report No.
Alexandra Wayllace, Ning Lu, Benjamin Mirus	

9. Performing Organization Name and Address	10. Work Unit No. (TRAIS)
Colorado School of Mines 1500 Illinois St. Golden, CO 80401	11. Contract or Grant No. 411013042

12. Sponsoring Agency Name and Address	13. Type of Report and Period Covered
Colorado Department of Transportation - Research 4201 E. Arkansas Ave. Denver, CO 80222	Final Draft
	14. Sponsoring Agency Code

15. Supplementary Notes

16. Abstract

A new methodology that uses recent advances in unsaturated soil mechanics and hydrology was developed and tested. The approach consists of using soil suction and moisture content field information in the prediction of the likelihood of landslide movement. The testing ground was an active landslide on I-70 west of the Eisenhower/Johnson Memorial Tunnels. A joint effort between Colorado School of Mines, CDOT, and USGS performed detailed site characterization, set up and calibrated a hydro-mechanical model of the site based on seven years of field data, and performed a stability analysis of the slope. Results indicate that consecutive years of high or low infiltration have a compounding effect so that the slope stability is influenced by the preceding years. Additionally, a new drainage system is proposed based on analysis of the current horizontal drains.

17. Keywords	18. Distribution Statement
Infiltration-induced landslides, unsaturated soils, CDOT	This document is available on CDOT's website http://www.coloradodot.info/programs/research/pdfs

19. Security Classif. (of this report)	20. Security Classif. (of this page)	21. No. of Pages	22. Price
Unclassified	Unclassified		

In-situ Monitoring of Infiltration-induced Instability of I-70 Embankment West of the Eisenhower-Johnson Memorial Tunnels, Phase III

Principal Investigator:
Dr. Alexandra Wayllace, Colorado School of Mines

Co-Principal Investigator:
Dr. Ning Lu, Colorado School of Mines

In collaboration with:
Benjamin Mirus, USGS Landslide Hazards Team

Submitted to:

Thien Tran, P.E.
e-mail: *Thien.Tran@state.co.us*
Research Engineer
CDOT-DTD Applied Research and Innovation Branch

2829 W. Howard Place

Denver, CO 80204

February 2021

ACKNOWLEDGEMENTS

The authors would like to thank the study panel members of the three phases of this project: Aziz Khan, Grant Anderson, Russel Cox, Matt Greer, Tonya Hart, Hsing-Cheng Liu, Amanullah Mommandi, William Scheuerman, David Thomas, Mark Vessely, and Trever Wang. We are also very thankful to the various CDOT and USGS personnel that provided very valuable input during the research progress meetings and site visits: Alfred Gross, David Novak, and Ty Ortiz. We are grateful for the technical review of this report provided by Emily Bedinger (USGS) and Thien Tran (CDOT). Most importantly, we would also like to acknowledge the hard work of the graduate student that worked on this project: Eric Hinds. Any use of trade, firm, or product names is for descriptive purposes only and does not imply endorsement by the U.S. Government.

EXECUTIVE SUMMARY

A joint effort between the Colorado School of Mines (CSM), the Colorado Department of Transportation (CDOT), and the Landslides Hazards Program of the United States Geological Survey was established to study the Straight Creek landslide, an active landslide on I-70 west of the Eisenhower/Johnson Memorial Tunnels, mileposts 212.0 to 212.1. Records indicate that during the past forty years the hillslope in this area has moved episodically causing more than 2 m of pavement settlement. A temporary solution was to level the road by adding asphalt to the area of settlement forcing to close at least partially the road on several occasions. Other efforts by CDOT to stabilize the site include installing horizontal drains and installing geofoam caissons on the affected stretch of I-70. Because it is located 3,240 m (10,630 ft) above sea level and surrounded by very steep terrain near the continental divide of the Rocky Mountains, the accessibility for heavy equipment is limited, and the permanent remedy cost is estimated to exceed $10 million. Such a remedial fix would necessitate closing the highway for an extended period, which is not practical due to heavy mountain traffic in this area.

This research had three phases: Phases I and II (2010-2016) characterized the site in detail, monitored groundwater table continuously, and identified the slide triggering mechanism as the interaction of rapid infiltration of spring snowmelt with site stratigraphy. This report presents the results of Phase III, which incorporated data from borehole logs, snow water equivalent sensors, rain gages, inclinometers, and piezometers, into a hydro-mechanical model. This model evaluates the effect on the stability of the Straight Creek slide of variability in infiltration characteristics and of remediation projects undertaken in 2011 and 2012.

Results indicate that there is a compounding effect of consecutive years of high or low infiltration on site hydrology, so that stability in a given year is influenced by the preceding years. Of those studied, the most important single-year atmospheric factor causing instability is the amount of snowmelt, followed by the rate at which it infiltrates; meanwhile, early partial snowmelt and summer rainfall are found to have a relatively negligible effect. The lightweight caissons installed in 2011 and 2012 are found to have no substantial effect on slide movement, as they reduce normal forces and frictional resistance along the failure surface as well as gravitational driving forces. The horizontal drains installed near the slide toe are found to reduce pore pressures and increase stability in a limited area due to the low conductivity of surrounding materials. Based on these analyses, a new drainage system is proposed and evaluated, which would be installed above the highway embankment in order to intercept groundwater before it encounters the conductivity contrast. Numerical modeling demonstrates that this design can improve the slope stability more effectively.

TABLE OF CONTENTS

1. INTRODUCTION AND BACKGROUND

Landslides on highway embankments and nearby hillslopes are common geologic hazards to transportation corridors in Colorado. Currently, the Colorado Department of Transportation (CDOT) has identified 124 such landslides, many of which move annually and are reportedly induced by infiltration of rainfall or snowmelt. When these slopes fail, they threaten public safety and private property, block highway traffic, and damage transportation infrastructure. Instability of these slopes in many cases results from infiltration of snowmelt and rainfall into variably saturated hillslope soil and rock materials. As water infiltrates into the soil, the water content and suction of the soil change and the water table position varies leading to a change in effective stress throughout the slope. These changes then drive changes in the stability of the slope. Estimates of the costs to reduce the risk to a moderate level often exceed tens of millions of dollars per slide, creating a strong public interest in maximizing the efficacy and minimizing the cost of interventions. Thus, it is important to understand the main mechanisms that affect the hillslope stability and the effects of intervention projects. With this goal, a joint effort between CDOT, the Colorado School of Mines (CSM), and the U.S. Geological Survey Landslides Hazard Program (USGS-LHP) was initiated in 2010 to investigate the Straight Creek landslide, an active landslide located in Summit County on I-70 west of the Eisenhower/Johnson Memorial Tunnels, mileposts 212.0 to 212.1.

The Straight Creek landslide, located on a steep south facing slope, is classified as “large” (width > 500 ft and depth > 50 ft) by CDOT and has experienced episodic annual movement since 1973. The relevant stretch of I-70 has an average daily traffic of over 20,000 vehicles and is important to the trucking and tourism industries because alternative routes are steep, narrow, and not viable for larger trucks. Large-scale remediation projects are not feasible because they would require closing the highway for an impractical amount of time. The embankment was constructed in the 1960s; shortly after, several landslides occurred, and Robinson & Associates was hired to perform a geotechnical investigation of the area (Robinson, 1971). In 1973, a bulge appeared near the eastbound lanes of the highway; soon after, downslope movement occurred, causing measurable road subsidence. The investigation identified excess pore water pressures as the cause of failure, and a draining system was installed about 2 m below the surface; unfortunately, this system was destroyed in 1979 during the widening of the embankment (Kumar & Associates, 1997). A

temporary measure to maintain a road leveled surface was asphalt capping; however, this measure was not efficient because it had to be done several times per year, causing partial road closures. In 1996, CDOT commissioned Kumar & Associates to perform a more detailed investigation. Their report indicates an ongoing slide failure, identifies the shear zone, and provides stratigraphic information from six boreholes drilled on the west and eastbound shoulders of the highway, as well as near the toe of the slide. In 2007 and 2008, CDOT installed inclinometers in the east and westbound shoulders of the affected I-70 stretch; the sensors maxed out within a year, measuring over 5 cm of lateral displacement. In 2011 and 2012, Shannon & Wilson, Inc. installed lightweight caissons in the highway, and ten horizontal drains near the slide toe, to decrease normal stresses on the failure plane and pore water pressures in the hillslope. Figure 1a portrays the slide location and extents.

The CSM-CDOT-USGS investigation was implemented in three phases. Phase I was an effort to understand the environmental setting and triggering mechanism of the failure, which included mapping of the failure zone, a subsurface investigation, and installation of sensors that have continuously monitored groundwater behavior and ground movements in the slope since 2011. Phase II aimed to fully understand the seasonal hydrology that leads to mechanical instability. All available information on stratigraphy, construction at this location, and known water table levels, was used to create an extended geological cross section of the entire watershed area and a conceptual model of the annual hydrology, which was incorporated into a 2-dimensional numerical model. The results of the hydrological model were then used in a preliminary slope stability analysis to assess the local factor of safety in the slope under the different hydrological conditions and confirm that movements in the slope are triggered by the large amount of infiltration into the slope during the spring season (CDOT report 2017-12). This report presents the findings of Phase III, which involves installing additional field instrumentation, gathering additional data on atmospheric and groundwater conditions, and extending stability analyses to consider the spatiotemporal evolution of instability using a local factor of safety concept incorporated into hydro-mechanical modeling. The purpose of Phase III is to resolve uncertainty about where the failure surface intersects the roadway, to characterize the effect on site hydrology and stability of annual variability and multi-year patterns in infiltration characteristics, to assess the impact of the

remediation work conducted in 2011 and 2012, and to propose and evaluate a new, more targeted remediation design.

The content of this report uses material published in the following documents:

i) Hinds, E. (2018). *Effects of atmospheric variability and remediation techniques on the stability of an interstate highway embankment*. M.S. Thesis, Colorado School of Mines: Golden, CO, 167 pp. https://hdl.handle.net/11124/172344

ii) Hinds, E., Lu, N., Mirus, B., and Wayllace, A. (2019). "Effects of Infiltration Characteristics on Spatial-Temporal Evolution of Stability of an Interstate Highway Embankment." *Journal of Geotechnical and Geoenvironmental Engineering*, 145(9): 05019008. https://doi.org/10.1061/(ASCE)GT.1943-5606.0002127

iii) Wayllace, A., Thunder, B., Lu, N., Khan, A., and Godt, J. W. (2019). "Hydrological Behavior of an Infiltration-Induced Landslide in Colorado, USA." *Geofluids*, 2019: 1959303. https://doi.org/10.1155/2019/1659303

iv) Hinds, E., Lu, N., Mirus, B. B., and Wayllace, A. (2021). "Effects of Infiltration Characteristics on Spatial-Temporal Evolution of Stability of an Interstate Highway Embankment." *Engineering Geology,* 2021: Volume 291, 106240. https://doi.org/10.1016/j.enggeo.2021.106240

2. RESEARCH TASKS

Five main tasks were identified during Phase III of this project:

Task I: Field monitoring continuation and improvement

Task II: Hydrological and slope stability analysis

Task III: Mitigation techniques evaluation

Task IV: Recommendations for site remediation

Task V: Draft report and final report

3. TASK I: FIELD MONITORING CONTINUATION AND IMPROVEMENT

3.1 Site description and instrumentation

The study site is located in Summit County on I-70 west of the Eisenhower/Johnson Memorial Tunnels, mileposts 212.0 to 212.1 (Figure 1a). At an elevation of approximately 3,252 m (10,670

ft) above sea level and with a roughly 30° inclination, the slide mass is approximately 175 m wide and 123 m long.

During Phase I and Phase II of this project, site characterization and instrumentation included drilling four boreholes, laboratory testing of shear strength and hydrological properties of relatively undisturbed samples, and installing 2 inclinometers and 4 vibrating wire piezometers. In Phase III, the data obtained from that instrumentation was monitored and analyzed; furthermore, four additional boreholes were drilled, and four vibrating wire piezometers were installed (Figure 1b). Logs from all boreholes conducted since 2010 as part of this investigation are included in Appendix A.

A two-dimensional soil profile along a centerline transect through the slide is shown in Figure 2; this information and the general characteristics of each material were derived from borehole logs from past investigations (Lovering, 1935; Robinson & Associates, 1971; Kumar & Associates, 1997; Thunder, 2016), core sample testing (Thunder, 2016), and the 4 boreholes drilled during the current study. The bedrock is primarily massive dark gneiss with occasional pegmatite and mica intrusions, which is mostly competent and relatively impermeable compared with overlying materials. The bedrock surface is generally parallel to the ground surface, although it is more steeply inclined towards the west in the western half of the slide. Overlying the competent bedrock is a layer of fractured and weathered material derived from the same dark gneiss, varying in thickness from 1 m to close to 30 m. The degree of weathering increases further down the slope; therefore, this layer was divided into two groups for the conceptual and numerical analysis. The first group, called fractured gneiss, is found on the slope above the embankment; it presents clean fracture surfaces with little weathering or infill and has high frictional strength and hydraulic conductivity. The second group, called decomposed gneiss, is found underneath the embankment and to the south of it. This material displays a higher degree of weathering, with lower strength and hydraulic conductivity than the fractured gneiss material. Surficial soil on the slope consists of colluvial deposits with angular, coarse sand to cobble-sized grains derived from the gneiss bedrock. Alluvial soil on the valley floor is more uniform, consisting of rounded sand-sized grains. Mechanical properties for the two materials are similar, but the hydraulic conductivity of the colluvium is higher due to a lower in situ density caused by depositional processes. The tunnel-

cuttings material used for embankment fill is extremely heterogeneous, including large rock fragments and boulders, construction rubble (such as decomposing timbers from shoring), and more fine-grained material than the surrounding native soils. Hydraulic conductivity of this material is very low due to this fines content. The embankment fill is approximately 14 m thick under the westbound shoulder of I-70, approximately 29 m thick under the eastbound shoulder, and extends approximately 61 m downslope (Hinds, 2018).

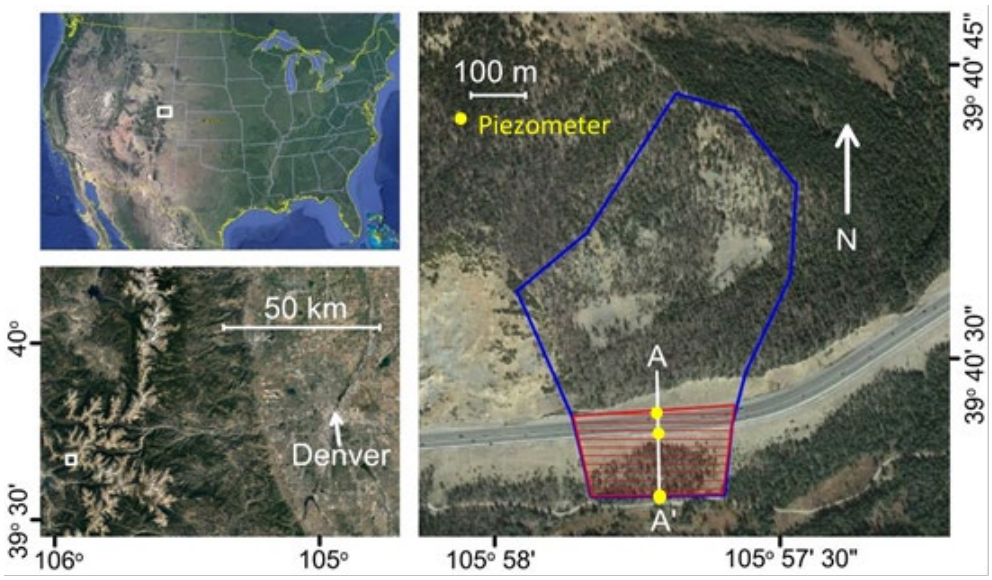

(a)

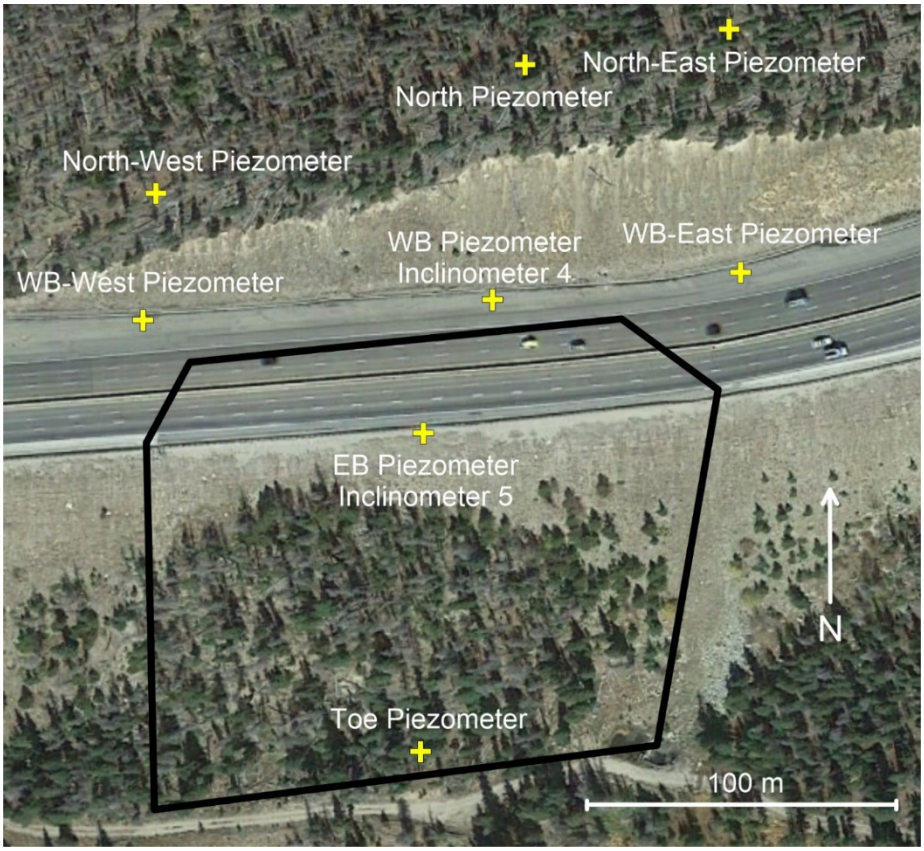

(b)

Figure 1. (a) Straight Creek slide location and extents; approximate slide area is shaded in red, approximate watershed area is outlined in blue and A-A' transect shown in subsequent figures. (b) Piezometer locations with approximate slide extents shown in black (from Hinds, 2018).

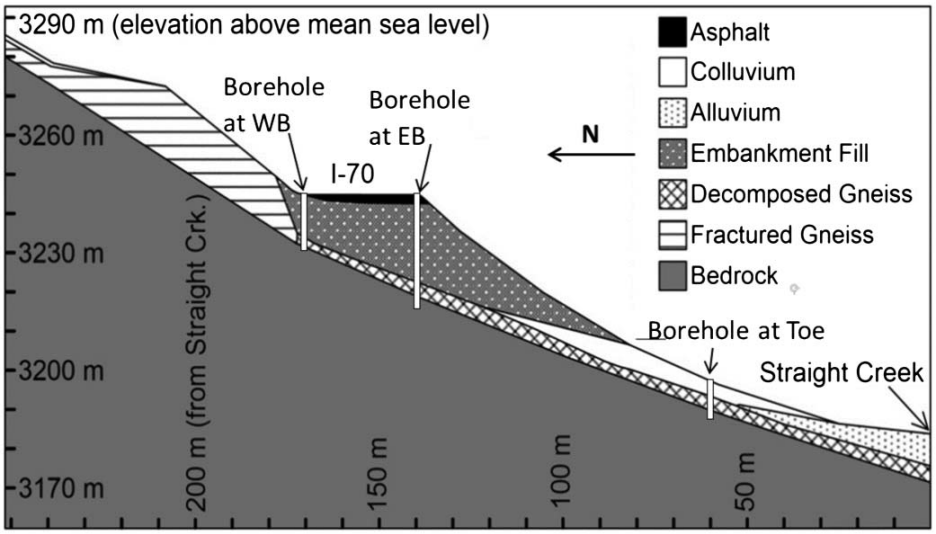

Figure 2. Transect showing subsurface material distribution along the slide centerline shown in A-A' transect in Figure 1 (from Hinds, et al., 2019).

3.2 Groundwater table variations

During the first and second phases of this project, it was clearly established that the hydrology of the hillslope, particularly the dynamic changes in the groundwater table, was a key factor in the stability of the slope (Wayllace et al., 2012, Wayllace et al., 2019).

Groundwater data in the first phase included the installation of three piezometers (P1, P2, and P3); it was then evident that to better characterize hydrologic behavior, more information was needed on the slope north of I-70, so a fourth piezometer (P4) was installed during Phase II. Four additional piezometers were installed over the summer of 2017; these were distributed laterally over the north slope. The depths below ground surface and installation date of all piezometers are provided in Table 1; the piezometers' locations are provided in Figure 1b. Piezometers P1 and P2 connected to a data logger near the toe of the slide, whereas piezometers P3-P8 connected to a data logger located on the Westbound shoulder of I-70. Interruptions in the data occurred sometimes over the winter season, as snow and deadfall often disrupt the cabled connections. The details on the installation of the equipment are provided in Appendix B.

Table 1. List of Piezometers, installation depth and dates.

Number	Name	Date Installed	Depth [m]
P1	WB	10/24/2011	17.4
P2	Toe	10/14/2011	9.0
P3	EB	8/9/2012	33.5
P4	North	4/7/2016	15.2
P5	WB-East	8/4/2017	34.0
P6	WB-West	8/4/2017	36.1
P7	North-West	8/4/2017	18.5
P8	North-East	8/16/2017	17.1

The data obtained with the piezometers is reported in Figure 3, where the ground water table (GWT) elevations are calculated based on the measured pressure head, the location of the instrument, and the installation depth. In general, the observations for piezometers P1-P3 are consistent with previous years: Groundwater table near the westbound shoulder (P1) varies eight to ten meters per year, while only ~30m across, near the eastbound shoulder, the variations of groundwater table (P3) are half as much (4m – 5m). Near the toe of the slide, water table variations throughout the year (P2) range between 1 m and 2 m. Measurements from the north area of I-70 are consistent with previous conceptual models (Wayllace et al., 2019); the water table varies from 1 m to 2 m throughout a year, confirming a material north of I-70 with larger hydraulic conductivity than the material underneath the highway.

In addition to the piezometer data, this study also used data obtained from a stream gage maintained by USGS; the stream gage, USGS 09051050, is located on Straight Creek approximately 7.8 km west-southwest from the slide site (Figure 4). Even though there are limitations on using this data, the base flow is generated by—and therefore a useful proxy for—groundwater levels.

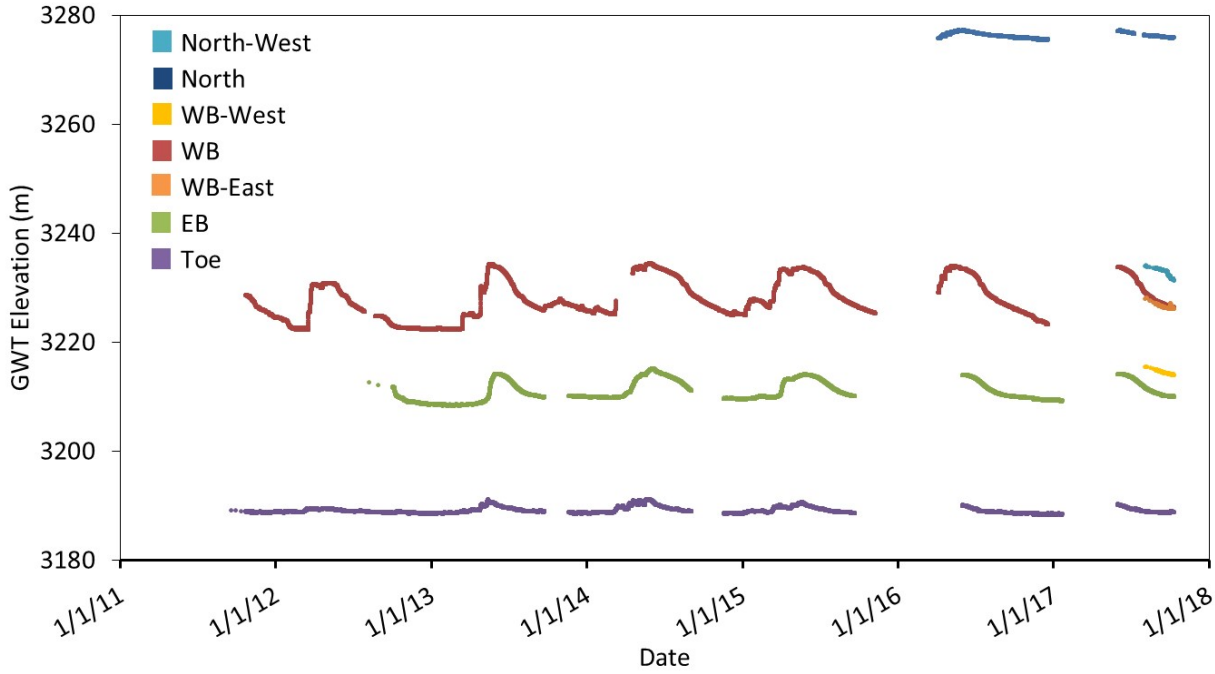

Figure 3. Groundwater level monitored at seven locations at the study site.

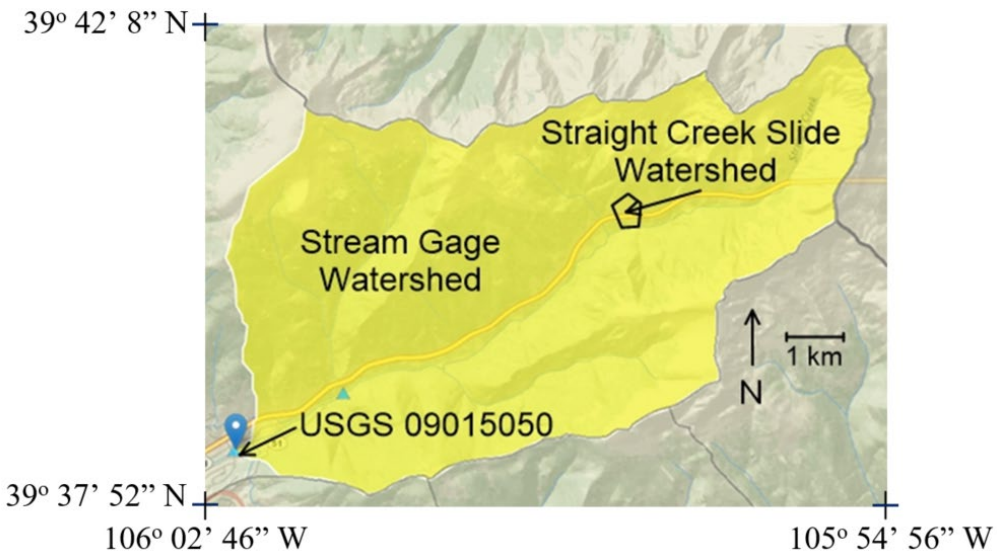

Figure 4. Location of USGS stream gage 09051050 (image modified from USGS Streamstats server; USGS StreamStats, 2018). Yellow shaded area is the drainage basin for this stream gage, and the area outlined in black is the slide area and its watershed (from Hinds, 2018).

Among the several methods available for calculating base flow from a stream hydrograph, this analysis uses a single-parameter digital filter implemented in the Web-based Hydrograph Analysis Tool (WHAT) created by Purdue University's College of Engineering (Lim et al., 2005). This

method assumes that high frequency waves in stream flow data can correspond with direct runoff and low frequency waves with base flow fluctuations. The filter is expressed as:

$$q_t = \alpha q_{t-1} + \left(\frac{1+\alpha}{2}\right)(Q_t - Q_{t-1}) \quad (1)$$

where q_t is the filtered direct runoff (i.e., the portion of stream flow that is not base flow) at time t, Q is the total stream flow, and α is the filter parameter, for which a value of 0.925 was used based on the findings and recommendations of Nathan and McMahon (1990). This filter method is sometimes referred to as the BFLOW filter, due to its use in the popular BFLOW software produced by the USDA Agricultural Research Service. Raw stream flow data and the filtered base flow for 2010 through 2015 are shown in Figure 5.

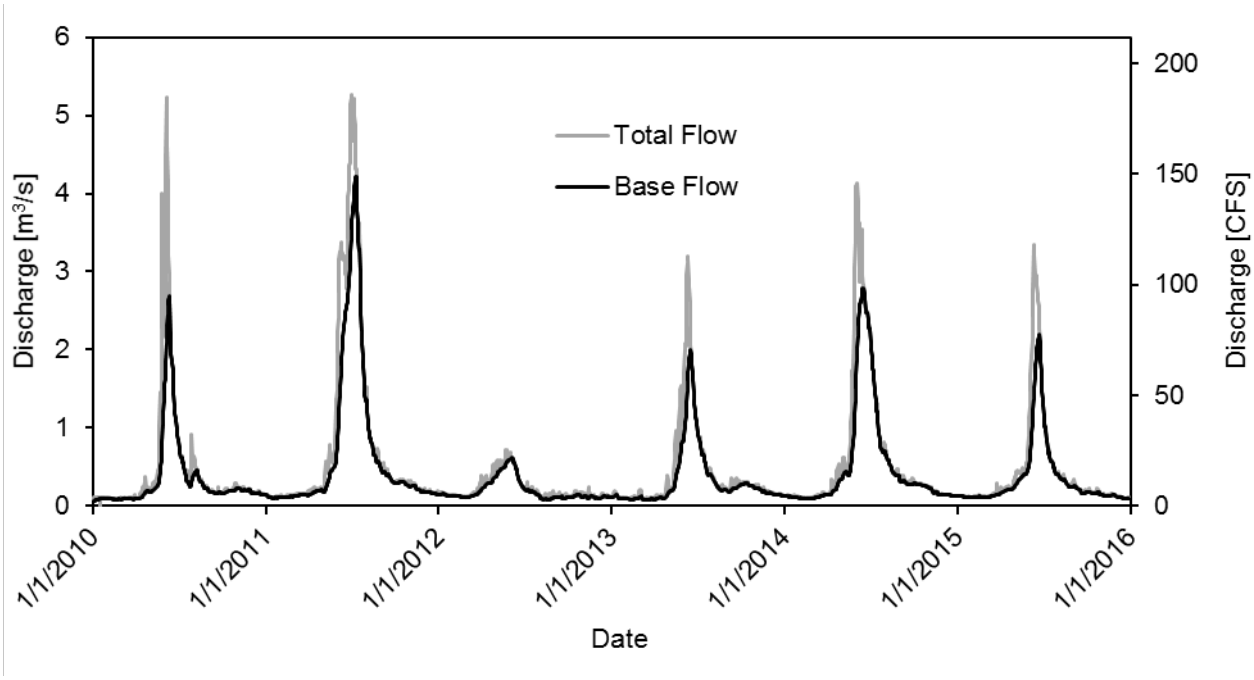

Figure 5. Total flow and filtered base flow at USGS stream gage 09051050, 2010 through 2015 (from Hinds, 2018).

The annual peak base flow levels fluctuate in a similar pattern to peak groundwater table elevations recorded by the CSM piezometers. In addition, as it is observed below, this pattern also matches the annual cumulative snowmelt infiltration amounts (Figure 6). The annual peak values for total (unfiltered) flow suggest that peak levels for 2010 and 2011 are equal, despite the fact that the cumulative snowmelt infiltration in 2011 is twice as high as in 2010. This suggests that the filtering method is achieving its purpose of extracting groundwater-derived flow from the discharge data, and that the calculated base flow is in fact a useful and valid proxy for groundwater levels.

3.3 Infiltration data

Atmospheric data in this study was obtained from the Grizzly Peak SNOTEL Station maintained by the Natural Resource Conservation Service (NRCS) of the US Department of Agriculture (NRCS, 2018). This station is located approximately 14 km to the southeast of the slide site, at a similar elevation and generally facing south. The information used include daily maximum air temperature, annual cumulative precipitation, and snow-water equivalent (SWE), which is a measurement of the weight of water contained within a snowpack, expressed as an equivalent height of liquid water. In this investigation, any negative change in SWE is interpreted as snowpack melting and assumed to directly infiltrate (defined as snowmelt infiltration). Any increase in cumulative precipitation occurring when SWE is zero (i.e., no snowpack existed) and temperatures are above freezing is assumed to also directly infiltrate (defined as rainfall infiltration), whereas precipitation occurring on a day with a non-zero SWE is assumed to either add to the snowpack or dissipate as runoff. These assumptions are consistent with field observations at the site.

SNOTEL data for infiltration due to rainfall and snowmelt for the years 1984 – 2017 is presented in Figure 6 and used to develop numerical model atmospheric inputs, to characterize the infiltration seasons, and to correlate with observed hydrologic response and slide activation. In general, infiltration cycles of an approximately 10-year period are observed, but also there are isolated years of elevated infiltration (2003, 2011). In addition, snowmelt infiltration exhibits greater magnitude and variation than precipitation infiltration, which lead to the hypothesis that the former is more important in causing slide activation.

It is important to point out limitations to the direct applicability of data collected at Grizzly Peak to the Straight Creek landslide; in addition to the distance between them, the Grizzly Peak site is topographically flatter, more heavily vegetated, and it does not face as directly south. Generally, this results in a later onset of snowmelt at Grizzly Peak than at the Straight Creek slide, as evidenced by the piezometer data (Figure 3). Thunder (2016) found that shifting the infiltration data two weeks earlier provided a modeled hydrologic response that better matched the observed

response; overall, however, the Grizzly Peak data is thought to provide a reasonably accurate measurement of atmospheric conditions at the Straight Creek slide site.

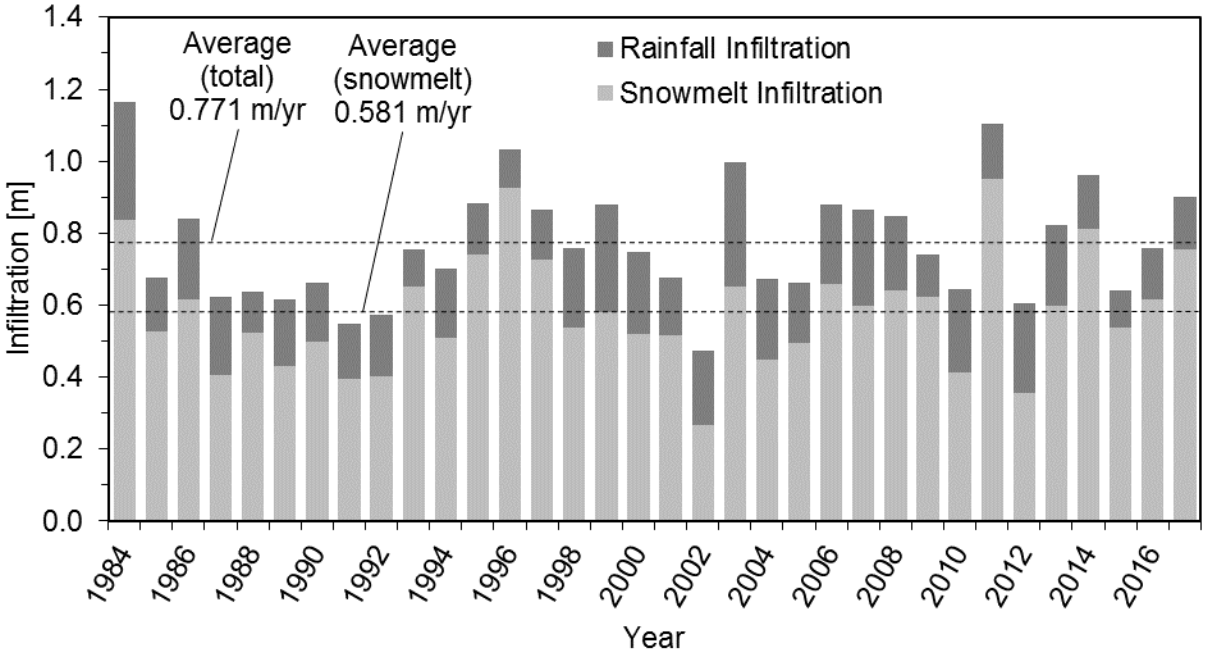

Figure 6. Infiltration totals calculated from SNOTEL data, 1984 through 2017 (from Hinds, 2018).

3.4 Slide Movement Data

Slide movement data include inclinometers installed at the site by CDOT, inclinometers installed by CDOT-CSM, and interviews with CDOT employees and contractors. Inclinometers installed by CDOT indicate that the failure surface is about 28 m (92 ft) below ground surface on the Eastbound shoulder, and about 20.7 m (68 ft) below ground surface on the Westbound shoulder. While informal interviews with CDOT employees indicate periods of increased movement in 1986 and 1996 through 1997, inclinometer data indicate more than 5 cm of lateral movement during both 1996-1997 and 2008-2009.

Figure 7 presents data of five inclinometers as follows: a) INC1 installed under the WB shoulder in 2007 by CDOT; this instrument was paved over in 2012; b) INC2 installed under the EB shoulder in 2008 by CDOT; c) INC3 installed under the WB shoulder in 2008 by CDOT; INC2 and INC3 measured approximately 5 cm of movement perpendicular to the highway within two years; d) INC4 installed on the WB shoulder in 2011 by CDOT-CSM; and e) INC5 installed under

the EB shoulder in 2012 by CDOT-CSM. INC4 and INC5 are still functional and measured a total displacement of less than 0.5 cm.

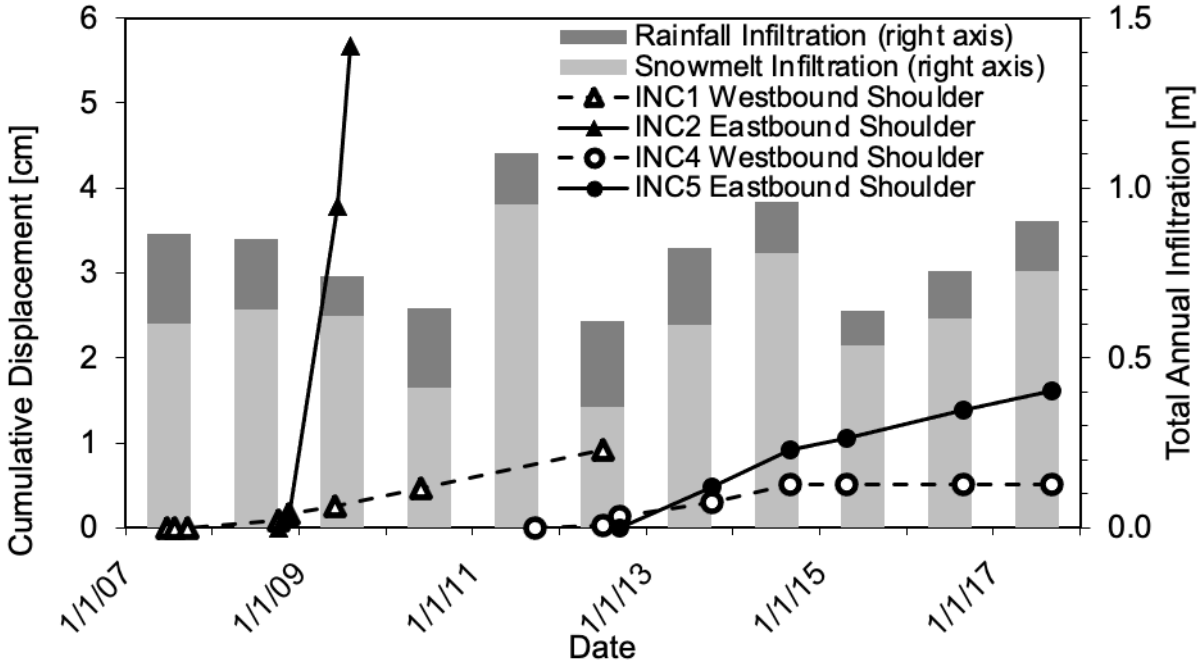

Figure 7. Inclinometer time series (data INC3 is nearly identical to data from INC2, and they are in similar locations; data from INC3 is not shown here) (from Hinds, 2018).

3.5 Failure surface

Based on the inclinometer readings presented in section 3.4 and on field observations, the failure plane of the landslide is believed to start near the westbound shoulder of I-70 and run along the decomposed gneiss-bedrock interface (Figure 8). This assumption is later supported by a numerical model that evaluates factor of safety at each point of the hillslope and thus allows the failure surface to develop based on the state of stress of each point instead of pre-assigning a possible failure surface.

4. TASK II: HYDROLOGICAL AND SLOPE STABILITY ANALYSIS

The contents of this section have been published in Hinds, et al. (2019).

4.1 Objectives

The questions addressed in this task are as follows:

A) How sensitive is embankment stability to annual variability in infiltration characteristics, including the total annual cumulative infiltration from snowmelt and rainfall, the rate at which that infiltration occurs, and variability in its timing?

B) Can infiltration conditions in previous years affect site hydrology and embankment stability during a given year?

C) Can infiltration characteristics be used to predict instability?

Because the landslide is a recurring failure that continually crosses between stable and unstable states, failing in essentially the same mode every year, albeit to varying degrees; a sensitivity analysis of the embankment's stability can help answer the questions above. This investigation develops an approach to quantify the controls on the activation length of recurring infiltration-triggered landslides and thereby identify physics-based thresholds for reactivation. The resulting insights contribute to understanding the specific trigger mechanisms and levels of risk for other similar sites.

4.2 Hydromechanical properties of site materials

Direct shear tests were performed on the samples to obtain strength properties. Transient Release and Imbibition Method (TRIM) (Wayllace and Lu, 2011) was used to obtain the hydrological properties. A mini-disk infiltrometer test was performed in the colluvium near the toe of the landslide to establish a range of in situ hydraulic conductivity. A slug test in the borehole north of I-70 (P4) provided an estimate of the saturated hydraulic conductivity (k_s) of the highly fractured gneiss. These values are reported in Table 1 along with other properties that have been provided by CDOT (Thunder, 2016).

Table 2. Hydro-mechanical properties of site materials (from Hinds, 2018).

	Soil-water retention properties [van Genuchten (1980) mode] (drying)				Saturated hydraulic conductivity,	Soil unit weight,	Cohesion,	Peak friction angle,	Elastic modulus,	Poisson's
Material	θ_r	θ_s	α	ν	k_s (m/day)	γ (kN/m^3)	c (kPa)	ϕ' (degrees)	E (kPa)	ratio, ν
Bedrock	0.06	0.34	1.374	1.72	0.001	23	5,638	56	5.3×10^7	0.30
Decomposed gneiss	0.065	0.41	7.5	1.89	1.06	22	25	38	50,000	0.25
Colluvium	0.08	0.33	2.35	2.12	6	20	0	34	50,000	0.25
Alluvium	0.07	0.33	2.35	2.12	3	20	0	30	50,000	0.25
Fractured gneiss	0.06	0.34	1.374	1.72	40	22	1,590	52	1.0×10^7	0.30
Embankment fill	0.08	0.33	1.374	2.12	0.5	21	25	35	30,000	0.25

4.3 Conceptual model of seasonal hydrology

The following conceptual model was presented in Phase II and consists of three seasonal stages (Lu et al., 2013). Stage I coincides with winter; in this stage the groundwater table is at its lowest level, resting along the surface of the competent bedrock. During this stage snowpack accumulates with essentially no melting or other infiltration occurring. Stage II corresponds to the spring; during this stage rapid melting of the snowpack occurs, and the meltwater begins to infiltrate into the hillslope. In most years, an initial fast increase in groundwater level is observed, probably due to snow plowed onto the WB shoulder melting as the temperatures warm up. Subsurface flow is initially perpendicular to the slope during this period because moisture gradients control flow direction more than gravity (simulated pathlines near the slope surface in Figure 8); as the slope becomes wetter, vertical flow predominates (simulated pathlines in the middle of the slope in Figure 8). Stage III corresponds roughly to summer and fall, when the hillslope has higher saturation and there is slower surface infiltration rate due to rainfall.

The hydrological observations at this site are unusual in that water table positions beneath the westbound shoulder of the highway (upslope) varied twice as much as water table positions beneath the eastbound shoulder (downslope), only 30m distant horizontally. This may be because the hydraulic conductivity contrast between the fractured gneiss and competent bedrock layers promotes lateral downslope flow along the bedrock interface north of I-70; this flow then encounters the contrast in hydraulic conductivity between the fractured gneiss and embankment material causing a rapid and pronounced elevation in groundwater levels underneath the westbound lanes of the highway.

As the groundwater rise increases pore water pressures along the failure surface, effective stress decreases or suction stress increases, resulting in shear strength reduction and slide activation. During the fall, precipitation slows, and the hillslope drains out and approaches the winter-steady state.

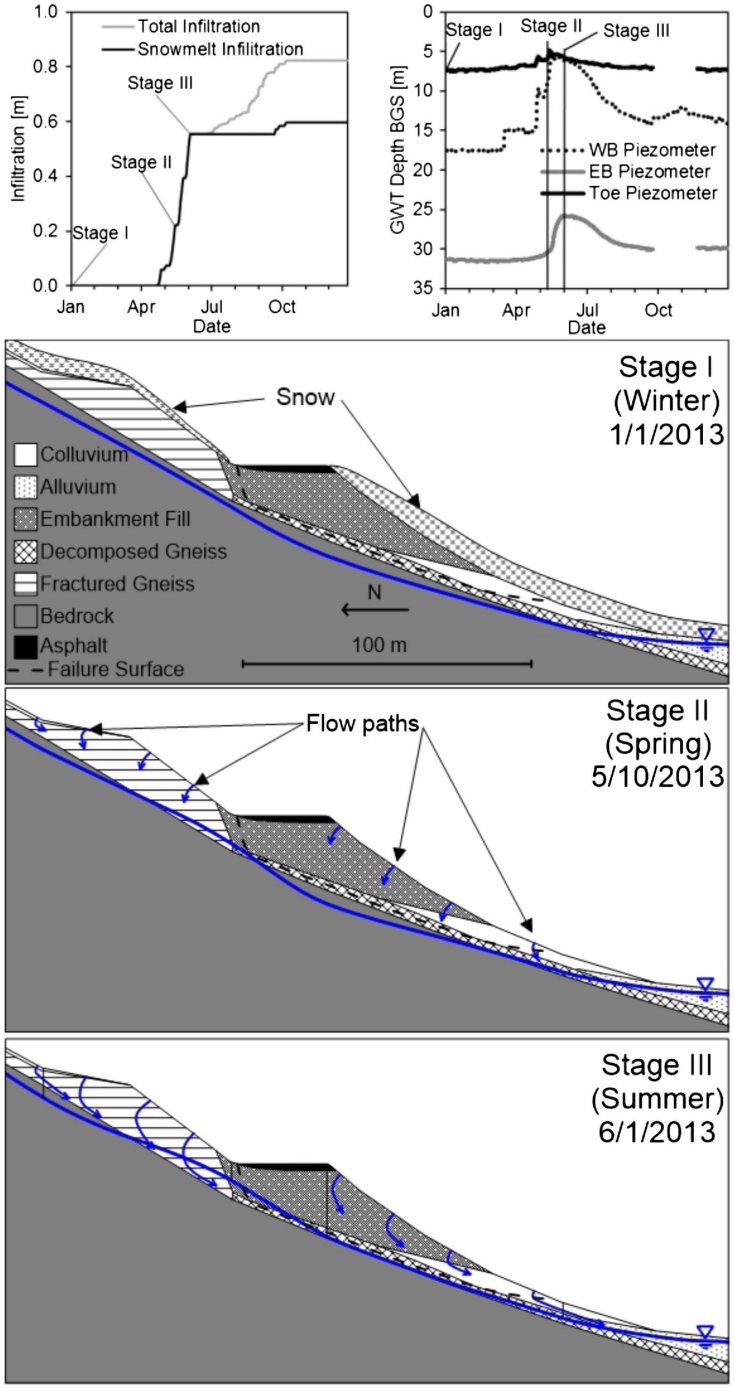

Figure 8. Infiltration data (top left) and piezometer data (top right) from 2013 linked to the conceptual model for seasonal hydrology: Stage I the water table (blue line) is initially below the failure surface; Stage II spring snowmelt infiltration causes the water table on the north side of the highway to rise, but it remains below the failure surface; Stage III continued infiltration causes the water table to rise further and intersect the failure surface (from Hinds et al., 2019).

4.4 Framework for numerical analysis

The hydro-mechanical framework used in this study was reported in Phase II. This rigorous, yet simple approach accounts for the major physical processes in the slope: stress, deformation, and variably saturated flow. In this framework, effective stress distributions used for the stability analysis are calculated throughout the slope by taking into account the slope's geomorphology, its hydrology, and the stress, strain, and deformation. The transient hydrological and mechanical behavior of the slope is analyzed by one-way coupling Richards' equation (2) with classical linear-elasticity equations.

$$\frac{\partial}{\partial x}\left[k_x(h_m)\frac{\partial h_m}{\partial x}\right]+\frac{\partial}{\partial y}\left[k_y(h_m)\frac{\partial h_m}{\partial y}\right]+\frac{\partial}{\partial z}\left[k_z(h_m)\left(\frac{\partial h_m}{\partial z}+1\right)\right]=C(h_m)\frac{\partial h_m}{\partial t} \tag{2}$$

where h_m is head, $k(h_m)$ is the hydraulic conductivity function (HCF), t is time, and $C(h_m)$ is the specific moisture capacity function, or the slope of the SWRC.

The effective stress $\boldsymbol{\sigma}'$ for variably saturated porous materials is defined as (Lu and Likos, 2004):

$$\boldsymbol{\sigma}' = \boldsymbol{\sigma} - \left(u_a + \sigma^s\right)\mathbf{I} \tag{3}$$

where $\boldsymbol{\sigma}$ is the total stress, u_a is the pore air pressure, $\mathbf{I}$ is the second-order identity tensor, and σ^s is the suction stress that is a characteristic function of saturation or matric suction and is expressed in a closed form for all soils (Lu and Likos, 2004, 2006):

$$\sigma^s = -(u_a - u_w) \qquad u_a - u_w \le 0 \tag{4a}$$

$$\sigma^s = -(u_a - u_w)S_e \qquad u_a - u_w \ge 0 \tag{4b}$$

where $(u_a - u_w)$ is the matric suction, and S_e is the equivalent degree of saturation. Using van Genuchten's model (1980) to describe the soil water retention curve, suction stress (equation (4b)) can be expressed as a sole function of matric suction (Lu and Likos, 2004; Lu et al., 2010):

$$\sigma^s = -\frac{(u_a - u_w)}{\left(1+\left[\alpha(u_a - u_w)\right]^n\right)^{(n-1)/n}} \tag{4c}$$

where α and n are empirical fitting parameters in van Genuchten's soil water retention model. Once the total stress, matric suction, and suction stress distributions throughout the slope are known, effective stress is calculated, and the stability of the slope can be calculated by taking into account the shear strength properties of the soil combined with the effective stress distribution.

Local factor of safety and Activated length

The hillslope stability was analyzed through a local factor of safety (LFS) method proposed in 2012 (Lu et al., 2013). Total stress field due to gravity and boundary conditions as well as changes in suction stress are used to calculate effective stress at each point in the slope. The local factor of safety is the ratio of the Coulomb stress and the current state of stress at each point in the hillslope (equation 5) and it is used for stability calculations (Figure 9). By similarity of triangles ACD and ABE, the LFS can be expressed conveniently in terms of the ratio of the adjusted mean stress of the current state of stress to the ac $LFS=\tau*/\tau$ stress of the potential failure state under the Mohr-Coulomb criterion. The Slope Cube module in Hydrus was used for these computations.

(5)

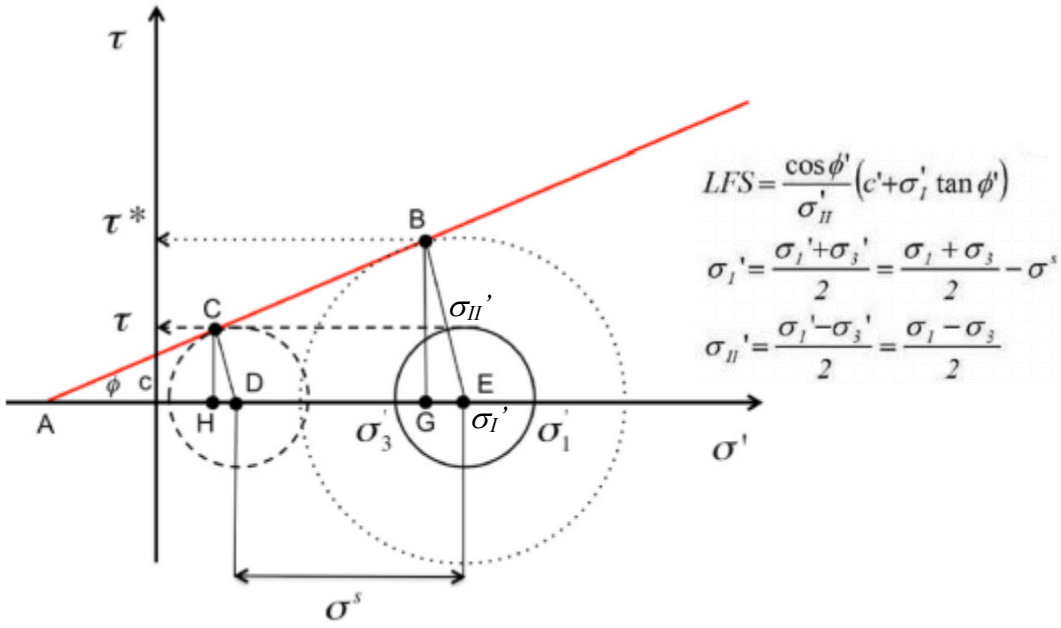

Figure 9. Conceptual illustration of the local factor of safety The current state of stress at any point in hillslope (shown as the solid-line circle) has a shear stress τ and shear strength τ*. The quantity τ*/τ can be used as an indicator of how far the current state of stress is from failure and is defined as the local factor of safety (LFS). If suction stress ss is reduced at this point, the circle shifts leftward and the LFS is reduced, indicating that the state of stress is closer to the failure condition or LFS = 1.0. (from Lu et al., 2013).

The concept of an activated length was used to assess the results of LFS analyses, whereby the length along an identified failure surface (derived from LFS contour plots) with LFS < 1 is expressed as a percentage of the full failure surface; a higher activated length indicates increased instability. Because the hydraulic conductivity of the embankment material is low and the seasonal patterns of pore-water pressure buildup are similar each year, for this model, the critical threshold

of activated length is identified by integrating the distribution of LFS over the identified failure surface and finding the activated length at which this integration is equal to zero. Strength parameters were adjusted so that this critical threshold (identified as 62.5% of the total failure length along the failure surface) is just reached at two points, with the lowest simulated instability corresponding to periods of known pronounced movement (the summers of 1986 and 2009).

4.5 Numerical model

The numerical model was conducted using HYDRUS 2D version 2.0 (Šimůnek et al., 2011), a finite-element software that models groundwater hydrology by solving Richards' equation (Richards 1931). Hydrological soil properties are described using van Genuchten (1980) Soil Water Retention Curve (SWRC) model and Mualem (1976) Hydraulic Conductivity Function (HCF) models. The Slope Cube module of HYDRUS 2D (Lu et al., 2016) is used for all stress field computation and stability analyses.

Model geometry was based on the transect in Figure 2, with the north boundary extended 740 m up to the watershed boundary (Figure 1); this large extent of northern slope is needed to generate the high lateral subsurface flux caused by infiltration over the entire slope up to the drainage divide. The south boundary is also extended 100 m to reduce boundary effects in stress calculations. The mechanical boundary conditions at both the north and south boundaries are no horizontal displacement but free vertical displacement. The mechanical boundary conditions at the bottom are no vertical displacement but free horizontal displacement. Based on site geologic and hydrologic conditions, the hydrologic boundary conditions are set to no flux at (1) the bottom and north boundaries due to the relative low hydraulic conductivity of the bedrock and intact rock, and (2) the highway surface due to the relative impermeable layer of asphalts. A specified flux boundary condition is used at the slope surface to allow applied infiltration for both rainfall and snowmelt precipitation. A constant head is applied at the south boundary to reflect the modulating effect of Straight Creek, which approximately coincides with that boundary. Although the water level of Straight Creek may vary, the annual fluctuation is less than a few feet or a meter. The effect of such change has a minimum effect on the groundwater table variation within the slope, as indicated in the recorded data nearby at the toe of the slope shown in Figure 3. Material properties reported in Table 2 were used.

Initial conditions were obtained by applying an average year of infiltration data created by distributing the average accumulated infiltration for both spring snowmelt and summer rainfall seasons over the average duration of these seasons. This gives rates of 0.0116 m/day during the snowmelt season, which runs from April 1 to May 21, and 0.00152 m/day during the rainfall season, which runs from May 22 to September 22. No infiltration is applied on the slope during all other periods of the average year. This infiltration cycle was then applied for 60 years, which is found to be sufficient for a steady cyclical state to be reached; this steady cyclical state was defined as one in which, under steady annually cyclical infiltration, peak and minimum pressure heads at the observation nodes do not change between years. This is therefore considered appropriate as a representative initial hydrologic conditions for investigating sensitivity to annual variability in infiltration. All model runs using these initial conditions begin on January 1.

The model was calibrated using the multiyear water table variation and the 2-week shift of infiltration boundary condition. Infiltration data for the years over which piezometer data are available; soil hydrologic properties and spatial distribution are then calibrated within ranges constrained by the literature, previous laboratory testing programs, and interpretation of borehole logs to match observed piezometer data as closely as possible. The hydrological simulation results are shown in Figure 10 indicating that the use of the SNOTEL infiltration with the two week shift is reasonable; the simulation and field measurements are closer to each other for the WB piezometer than for the piezometers at the EB and near the toe of the slide. Annual peak pressure heads, which are considered the most critical hydrologic result because they directly cause peak instability, generally match piezometer data very well, as do annual minimum pressure heads; the timing of pressure head change does not. Some discrepancy may be explained by differences between the Straight Creek slide site and the SNOTEL station site, which is 14 km away in a different (although similar) watershed, and in a location that is topographically flatter, more heavily forested, and more distant from roadways than the Straight Creek slide. These differences may be sufficient to cause the persistent disparity in timing and occasional disparity in magnitude of groundwater level peaks.

The Mohr-Coloumb failure criterion is used to represent the shear strength of the slope materials. The LFS distribution in the hillslope at critical state is provided in Figure 11. The calculated activated length for this condition is 62.5%.

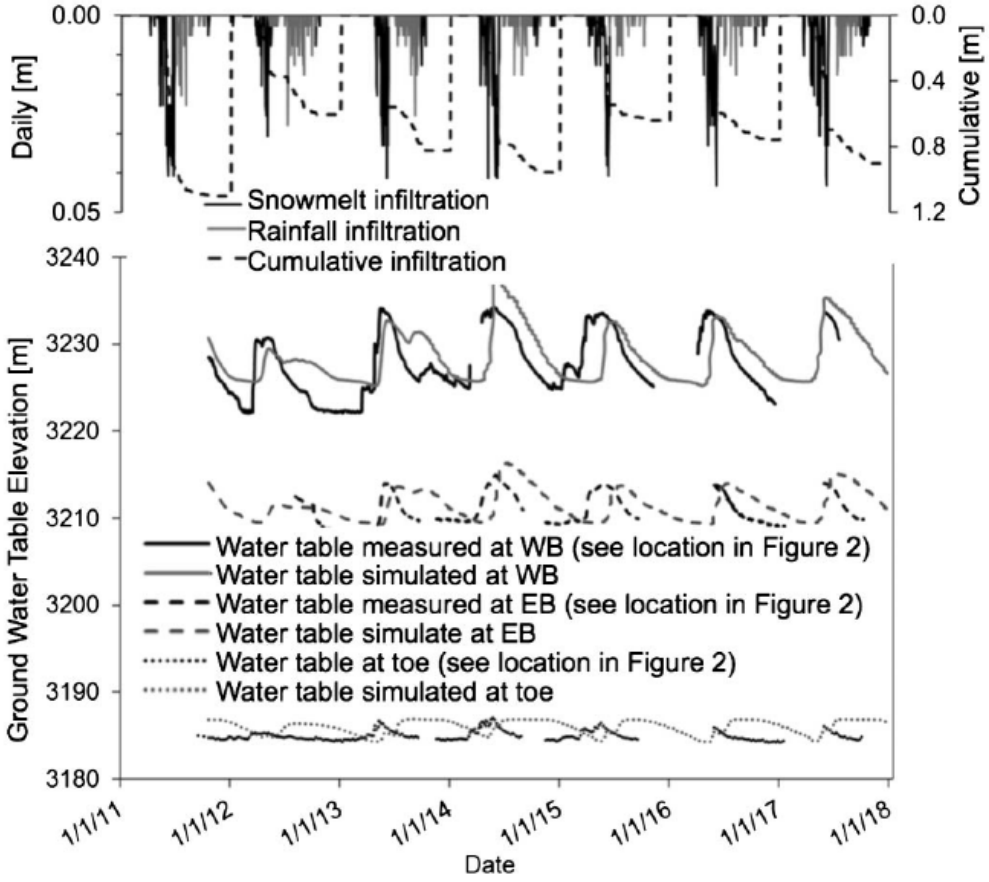

Figure 10. Measured and simulated groundwater table elevations and infiltration data, 2011-2018 (from Hinds et al., 2019).

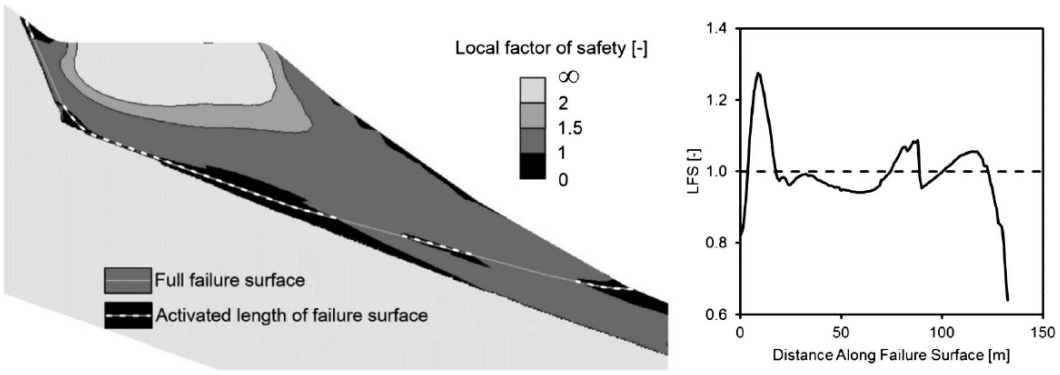

Figure 11. LFS contour map of embankment at critical state, showing activated length concept and distributions of LFS over the failure surface (from Hinds et al., 2019).

4.6 Sensitivity of Slope Stability to Annual Infiltration Characteristics

Annual cumulative infiltration from 1984 to 2018 is presented in Figure 12, and general infiltration characteristics are reported in Table 3. In every year on record, cumulative snowmelt infiltration is both much greater in magnitude (average of 0.581 m annual cumulative snowmelt infiltration versus 0.190 m annual cumulative rainfall infiltration) and occurs over a much shorter timescale (average duration of 45 days for snowmelt season versus 116 days for rainfall season). This suggests that snowmelt characteristics likely have a larger effect on embankment stability than rainfall. Years of above-average annual cumulative snowmelt infiltration coincide with known periods of pronounced slide movement and with higher modeled instability (Figure 12). There are years of above-average annual cumulative snowmelt infiltration and high-modeled instability for which pronounced movement is not noted (1984, 1993, 2003, 2006, 2007, and 2011); however, these years all occur during periods without inclinometer or continuous piezometer data. It is possible that little movement occurred despite high infiltration and pore pressures; informal interviews may have simply failed to record pronounced movement during these years, or extensive roadwork in 2011 may also have obscured pronounced movement during that year.

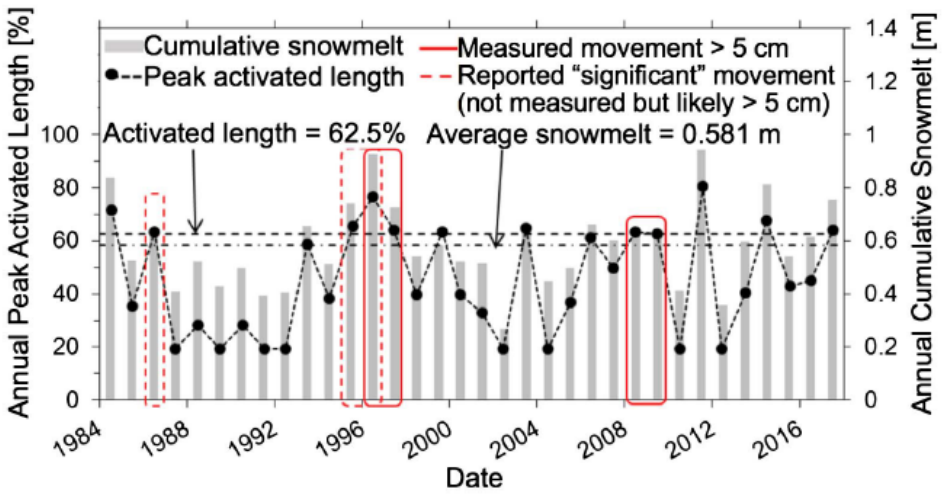

Figure 12. Annual cumulative infiltration, modeled annual peak activated length, and periods of known pronounced movement, 1984-2018 (from Hinds et al., 2019).

Table 3. Infiltration characteristics.

		Snowmelt Infiltration	Rainfall Infiltration	Total Infiltration
Average [m]		0.581	0.190	0.771
Minimum [m]		0.267	0.102	0.475
Maximum [m]		0.953	0.345	1.166
Standard Deviation	[m]	0.159	0.061	0.162
	[%]	27.3%	32.4%	21.0%

The rate of infiltration may have an effect on instability independent of the depth of cumulative infiltration. For a given depth of cumulative infiltration, a higher rate of infiltration creates higher subsurface flux (for a shorter duration), which exacerbates the pressure head increase at the hydraulic conductivity contrast at the embankment's upslope boundary. This compounding effect of infiltration rate is possibly evident in Figure 12: 1986, a year of known pronounced movement, had slightly higher than average cumulative annual snowmelt infiltration but had the third highest rate of snowmelt infiltration on record (17.6 mm/day, compared with average and maximum rates of 12.9 and 21.8 mm/day, respectively). Correlations between annual infiltration characteristics and annual peak pressure heads measured by piezometers strengthen the hypothesis that annual cumulative snowmelt infiltration and rate of snowmelt infiltration are the most important drivers of pressure heads beneath the embankment [and therefore of slide movement (Figure 13)]. Annual cumulative snowmelt infiltration and rate of snowmelt infiltration both have fairly strong positive correlations with annual peak pressure head at the WB piezometer (under the westbound shoulder), and weaker, less positive correlations with annual peak pressure head at the EB piezometer (under the eastbound shoulder). This is due to the attenuating effect of the low hydraulic conductivity materials within and beneath the embankment. As shown in Figure 13, all rainfall characteristics have very weak or nonexistent correlations with peak pressure heads, confirming that rainfall is essentially unrelated to embankment stability. This is because rainfall infiltration spreads over much longer period of time (May to October) than snowmelt (in a month or so in April).

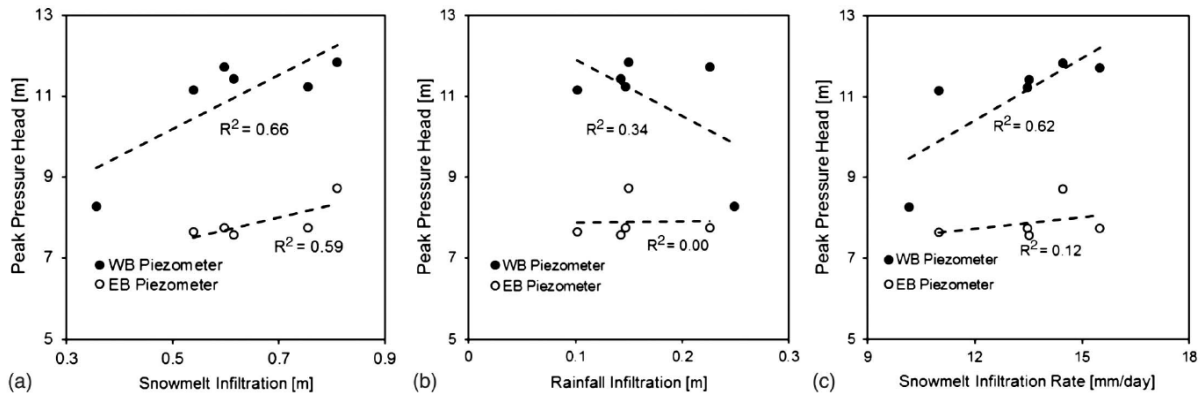

Figure 13. Correlations between annual peak pressure heads and (a) annual cumulative snowmelt infiltration; (b) annual cumulative rainfall infiltration; and (c) seasonal snowmelt infiltration rate (from Hinds et al., 2019).

Sensitivity to annual cumulative snowmelt and rainfall infiltration using numerical modeling was done by preparing twenty-five infiltration scenarios. Five cumulative annual infiltration amounts for each type of infiltration covering the range of observed values are given in Table 4. All possible combinations of these values for snowmelt and rainfall infiltration result in the 25 scenarios for cumulative annual infiltration amounts, which are then distributed over a time period typical for each infiltration scenario, i.e., April 1 to May 21 for snowmelt infiltration and May 22 to September 22 for rainfall infiltration, meaning that the infiltration rate varies. The infiltration data created by distributing a depth of cumulative infiltration over a typical duration are referred to as a generalized year to differentiate it from the use of daily infiltration data calculated directly from SNOTEL data. Each of the resulting 25 possible combinations of snowmelt and rainfall infiltration are then modeled, and the resulting activated length (LFS < 1 along typical failure surface) for each combination is used to produce a contour plot (Figure 14). The range of observed annual cumulative snowmelt infiltration can change the activated length by 60% of the full failure surface, whereas the range of observed annual cumulative rainfall infiltration can only change the activated length by 3.7% of the full failure surface (for an average value of annual cumulative snowmelt infiltration). The large activated length of the failure surface due to the snowmelt infiltration is because that snowmelt infiltration occurred during a much shorter period of time than the rainfall infiltration; the former occurred in days, and the latter occurred over many months. Because rainfall is shown to be relatively unimportant to embankment stability, the effect of infiltration rate is only studied for snowmelt infiltration. The same five levels of annual cumulative snowmelt are

modeled at five different levels of snowmelt infiltration rate (Table 4), requiring the duration to vary as well, and the resulting activated length for each combination is used to produce a contour plot (Figure 14b). For the average value of annual cumulative snowmelt infiltration, the range of observed snowmelt infiltration rate can change activated length by 29% of the full failure surface, substantially more than the maximum effect from rainfall infiltration.

In approximately two-thirds of the years on record, the main snowmelt season is preceded by an early partial snowmelt event. These events involve an average of 0.033 m of snowmelt infiltration, last for 1–2 weeks, and occur up to 2 months earlier than the onset of the main snowmelt season. Small pre-wetting events like this have in the past been found to accelerate and increase downslope subsurface flow (Whipkey, 1969; Lu and LeCain, 2003) by bringing hydraulic conductivity of subsurface materials closer to maximal, saturated values. The simulations were conducted to examine if these aforementioned pre-wetting events have more significant effects in the high hydraulic conductivity materials in the northern slope than in the low-hydraulic-conductivity materials within and beneath the embankment. If so, these pre-wetting events could exacerbate seasonally destabilizing pressure head increases by increasing the hydraulic conductivity contrast. However, it was found that early partial snowmelt events actually have a mitigating effect, allowing pressure heads to dissipate more quickly due to increased saturation of the low-hydraulic-conductivity materials.

This mitigating effect is not substantial; the greatest decrease in activated length due to early partial snowmelt is about 1%. Of all the infiltration characteristics studied, annual cumulative snowmelt infiltration is the most important driver of hydrology and instability. Its effect on the activated failure surface length is multiple times greater than that of any other factor. The rate at which snowmelt infiltrates is the second most important factor because it can substantially change activated failure surface length for a given depth of annual cumulative snowmelt infiltration; all other factors studied are essentially negligible. The effect of snowmelt characteristics is dominant because for the particular climate of this site, snowmelt is greater in quantity and rate than rainfall.

Table 4. Cumulative infiltration levels used in modeling synthesis (from Hinds et al., 2019).

Infiltration characteristic	Level 1 (minimum)	Level 2	Level 3 (average)	Level 4	Level 5 (maximum)
Annual cumulative rainfall (m)	0.102	0.146	0.190	0.268	0.345
Annual cumulative snowmelt (m)	0.267	0.424	0.581	0.767	0.953
Snowmelt infiltration rate (mm/day)	7.7	10.3	12.9	17.4	21.8

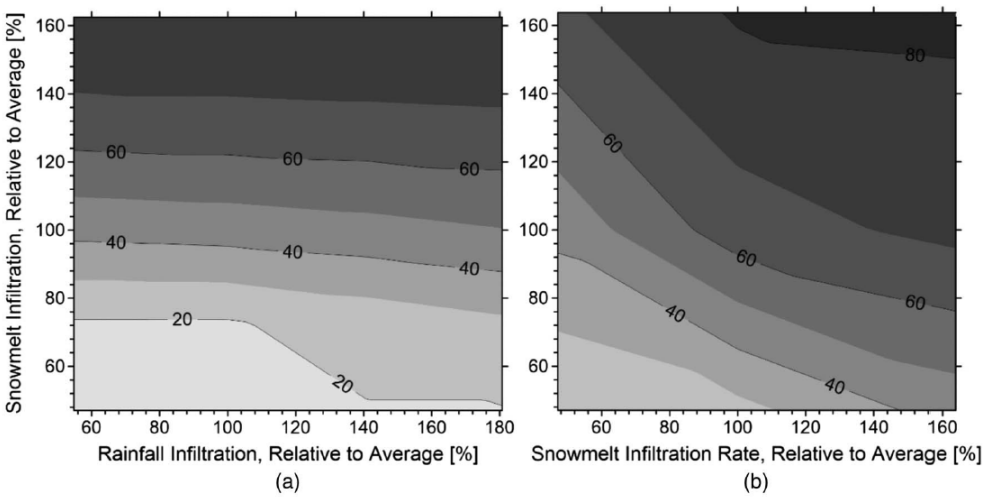

Figure 14. Contour plots of activated length modeled for various combinations of annual cumulative snowmelt infiltration and (a) rainfall infiltration; or (b) snowmelt infiltration rate (from Hinds et al., 2019).

4.7 Sensitivity of Slope Stability to Infiltration in Preceding Year

The effect of antecedent soil-moisture conditions on slope stability during infiltration has been firmly established; long-term (seasonal to annual scale) conditions have also been identified as particularly important (Campbell, 1975). Periods of known pronounced movement of the Straight Creek slide tend to coincide not only with years of above-average annual cumulative snowmelt infiltration, but also with periods of such years occurring consecutively (Figure 12). This suggests that pre-snowmelt groundwater levels may be affected by infiltration in the previous year; a year of above-average annual cumulative snowmelt infiltration may produce increased soil moisture that does not drain out to the same state as after a year of average or below-average annual cumulative snowmelt infiltration. This increase in antecedent soil-moisture conditions or groundwater level, referred to as a carryover effect in soil moisture, may amplify the seasonal

increase in pressure heads following snowmelt infiltration, as reported in some other studies (e.g., Wieczorek and Glade, 2005).

The period for which piezometer data are available is too short to conduct a rigorous analysis of this possible carryover effect. To expand the number of years available for analysis, a different measure of or proxy for groundwater levels is necessary; data from USGS Stream Gauge 09051050 (USGS, 2018) was used for this purpose, as explained in Section 3.2 of this report. The average subsequent winter base flow and minimum subsequent winter base flow can then be correlated to annual cumulative snowmelt infiltration; winter is defined as December 1 through March 31 for this analysis. There is in fact a positive correlation between the snowmelt infiltration in a given year and the base flow during the following winter (Figure 15). This correlation cannot completely explain variation in wintertime base flow, but it could explain much of the variation. Some discrepancy may be explained by the distance of both the stream gauge and SNOTEL site from the slide, and by the drainage area of the stream gauge, which is much larger (47.7 versus 0.3 km^2) and more varied than the slide site watershed.

If the assumption that changes in base flow correspond to changes in groundwater level is valid, then the proposed carryover effect seems likely to exist to some degree. The effect of infiltration history is modeled using daily infiltration data for 2009, 2008, 2001, and 2002; annual totals for these years and the 1984–2017 averages are presented in Table 5. The year 2009 had slightly higher than average annual cumulative snowmelt infiltration, one of the lowest values for a year of known pronounced movement and was preceded by a year (2008) of higher annual cumulative snowmelt, which resulted in an activated length of 62.5%. Because this is the lowest annual peak activated length for any year of known pronounced movement (also simulated for 1986, another year of known pronounced movement and slightly higher-than-average annual cumulative snowmelt infiltration), it is considered a threshold for elevated instability. By modeling 2009 as preceded by years of lower-than-average annual cumulative snowmelt infiltration (2001 and 2002), the effect of infiltration history on the development of instability is demonstrated.

When preceded by 2001 or 2002, the annual peak activated length simulated in 2009 is reduced to 57.9% or 52.0%, respectively (Figure 16). The reduction in peak activated length by up to 10.5%

of the full failure surface is potentially enough to substantially reduce or even eliminate movement in 2009 (Figure 12); this effect from the preceding year's infiltration is greater than that of annual cumulative rainfall infiltration for the Straight Creek site. The duration of the peak in activated length is also affected by the preceding year; for a year in which peak activated length will exceed 62.5% regardless of infiltration in the previous year, the period of time for which it will exceed this threshold will be responsive to this infiltration history. It is reasonable to expect that a longer period above this threshold will result in greater magnitude of slide movement. It was found that infiltration during the preceding year has a moderate but clear carryover effect on the hydrology and stability of the Straight Creek slide. Years of above-average annual cumulative infiltration increase groundwater levels at the onset of snowmelt in the following year, increasing the resultant peak pressure heads. Meanwhile, years of below-average annual cumulative infiltration have the opposite effect. The ability of the numerical model to simulate the importance of antecedent infiltration also corroborates the validity of the identified threshold of the failure length for landslide reactivation.

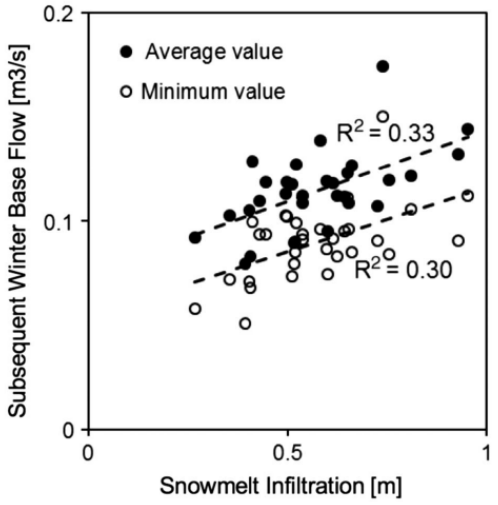

Figure 15. Correlations between infiltration and base flow in the subsequent winter season (from Hinds et al., 2019).

Table 5. Infiltration characteristics for 2009, 2008, 2001, and 2002 (from Hinds et al., 2019).

Year	Snowmelt infiltration (m)	Rainfall infiltration (m)	Total infiltration (m)
Average	0.581	0.190	0.771
2009	0.625	0.117	0.742
2008	0.643	0.203	0.846
2001	0.516	0.163	0.678
2002	0.267	0.208	0.475

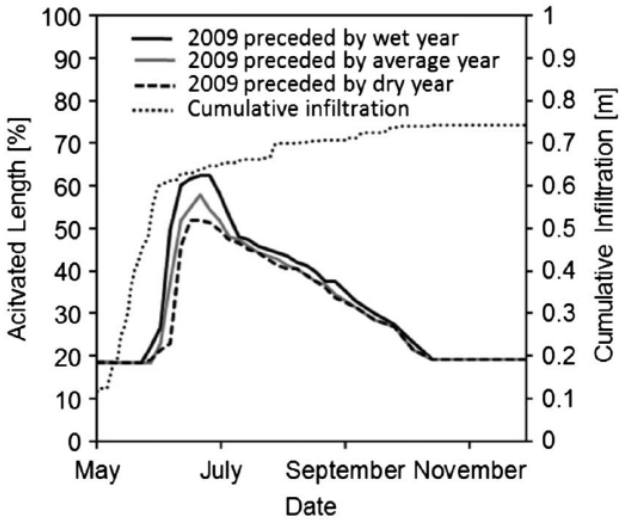

Figure 16. Activated length time series from 2009, modeled as preceded by different years (from Hinds et al., 2019).

4.8. Development of a Predictive Framework for Instability Threshold

The preceding sections demonstrate that annual cumulative snowmelt infiltration, rate of snowmelt infiltration, and annual cumulative infiltration in the preceding year are all important factors behind instability each year. This suggests the possibility of developing thresholds of combinations of these factors, above which pronounced movement is likely. These thresholds could aid CDOT in allocating resources to monitor for and rapidly address issues caused by increased movement. To set these thresholds, each year of available SNOTEL data (1984 through 2017) is modeled separately, preceded by years of different annual cumulative snowmelt infiltration. These preceding years were created by multiplying daily infiltration rates for a year of average annual cumulative snowmelt infiltration (1999) by a factor to match annual cumulative snowmelt infiltration to the levels specified in Table 4. Level 1 therefore represents a preceding year of

minimal annual cumulative snowmelt infiltration, Level 5 a preceding year of maximal annual cumulative snowmelt infiltration, and Levels 2 through 4 distributed evenly within the observed range. The resulting activated length is then compared with the minimum activated length corresponding to pronounced movement, which was set equal to the activated length modeled for 1986 and 2009 when all years were modeled sequentially (as in Figure 12). This is the lowest activated length modeled for a year of known pronounced movement. The threshold for infiltration that will likely cause this activated length can then be drawn between model cases that did or did not exceed it (Figure 17a), disregarding outliers as needed. These thresholds for each level of annual cumulative snowmelt infiltration in the preceding year can then be combined (Figure 17b).

Predicting snowmelt rate is not as straightforward as predicting annual cumulative snowmelt infiltration, which can be accurately estimated from SWE values preceding the main snowmelt season (which typically begins in April or early May). There are no clear correlations between temperature and snowmelt rate that apply across all years, even controlling for annual cumulative snowmelt infiltration. However, there are 11 identifiable cases of years with annual cumulative snowmelt infiltration within 5 mm of each other, nine of which have an identifiable difference in snowmelt rate. Of the nine cases, eight can be explained by the onset of snowmelt, and nine can be explained by the average temperature during the 45 days following the onset of snowmelt. Later onset, closer to early May than mid-April, coincides with high average temperatures in the subsequent snowmelt season and a faster snowmelt rate. These observations can be used as rough guides for estimating snowmelt rate, similar to the approach proposed by Chleborad (1998). Quantifying the Straight Creek slide's sensitivity to infiltration characteristics may therefore prove to not only add to the general body of knowledge related to infiltration-induced landslides, but also to provide practical benefits to CDOT in managing the risks of this slide. Through the use of this predictive framework, it may be possible to anticipate pronounced movement based on infiltration in the previous year and predicted annual cumulative snowmelt infiltration and snowmelt infiltration rate in the current year. This also represents a contribution toward developing hydro-meteorological thresholds based on the physical processes driving landslide initiation or reactivation (Bogaard and Greco, 2018; Mirus et al., 2018a, b; Thomas et al., 2018).

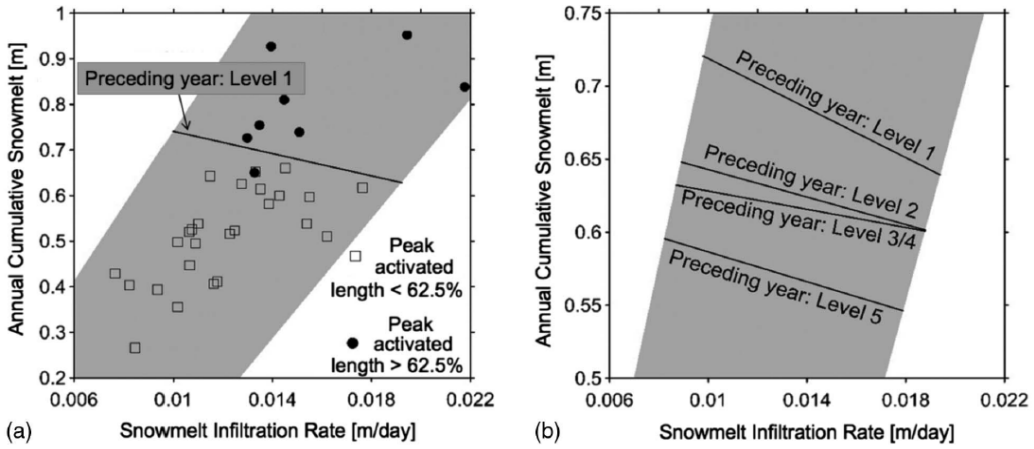

Figure 17. (a) Predictive framework development; and (b) final thresholds. Shaded area indicates region of observed data (from Hinds et al., 2019).

4.9. Main conclusions from Task II: Hydrological and slope stability analysis

This investigation has provided valuable insights into the particular subsurface stratigraphy and watershed hydrology that have led to instability at the Straight Creek landslide for 4.5 decades, while also adding to the body of general knowledge on infiltration-induced landslides and the effects of changes in the unsaturated zone on slope stability. This study uses LFS methodology to investigate the spatial-temporal evolution of slope failure and characterize the slide's sensitivity to single-year and multiyear variability in infiltration. The following conclusions can be drawn:

- Instability at this site is directly triggered by an abrupt dramatic seasonal increase in pore pressure beneath the embankment, which is caused by the rapid infiltration of snowmelt.
- Of the infiltration characteristics studied, annual cumulative snowmelt infiltration is by far the most important single-year factor in the level of slide activation and is likely sufficient to determine whether the slide will move and by how much in a given year.
- The rate at which snowmelt occurs also has a substantial effect on stability, although less so than the total amount of snowmelt. A faster rate of snowmelt exacerbates the seasonal increase in pressure head beneath the embankment, which is the cause for instability. All other single-year factors, such as summer season rainfall infiltration, are essentially negligible in comparison with the cumulative annual snowmelt and snowmelt rate.

- Slope stability can be affected by infiltration in the previous year. Consecutive years of high infiltration can have a compounding effect, increasing the magnitude of seasonal pressure head rise and result in less stability than single, isolated years of high infiltration. Likewise, consecutive years of low infiltration can suppress groundwater response to infiltration and increase slope stability in subsequent years. The case study illustrates that the effects of infiltration characteristics, namely annual snowpack accumulation, forecasted snowmelt rate, and the previous year's snowmelt, can be used to form tools for predicting increased movement of the Straight Creek slide in a given year. This method of developing instability threshold may be applied to other sites once the physical processes underlying the evolution of instability are understood.

5. TASK III: MITIGATION TECHNIQUES EVALUATION

The contents of this section have been published in Hinds (2018) and Hinds, et al. (2021).

5.1 Objectives

The 2-mile stretch of the I-70 corridor immediately west of the Eisenhower/Johnson Memorial Tunnels has been the subject of multiple geological investigations due to observed hillslope failures since the construction of the highway in the late 1960s. At the Straight Creek landslide, two remediation designs were applied: installing lightweight caissons beneath the highway surface, and installing horizontal drains near the toe of the landslide.

This task aims to answer the following questions:

a) What were the effects of the lightweight caissons installed in 2011 and 2012?
b) What were the effects of the ten horizontal drains installed in 2012?
c) What would be the potential effects of a proposed drain system installed north of I-70?

5.2 Effect of the lightweight caissons

The caissons were installed by Shannon and Wilson under the westbound lanes in 2011 and under the median and eastbound lanes in 2012. They are 1.5 m in diameter, 6.1 m deep except under the middle and right westbound lanes where they are 3 m deep and spaced 3 m on center in seven lines running parallel to the highway. The unit weight of the lightweight concrete is 5.7 to 6.1 kN/m^3 (36 to 39 PCF), in contrast to the estimated unit weight of 21.1 kN/m^3 (134 PCF) for the embankment fill. The volume of all caissons accounts for approximately 1.2% of the total slide mass volume and approximately 3.1% of the volume of the portion of the slide mass directly underneath the highway. This represents a weight reduction of 0.9% of the total slide mass and 2.2% of the portion of the slide mass directly underneath the highway. The intent behind the caisson design was to reduce the driving force, namely gravity, causing the slide, but the total change in slide mass was relatively modest.

During Phase II of this study, the stability modeling did not find a strong effect on slope stability from the caissons. Global factor of safety for groundwater levels representative of each season in the conceptual model were obtained using an extended version of the modified Bishop's method

of slices, which accounts for suction stress as per Lu and Godt (2013), in RocScience Slide 6.0 (Table 7). The effect of the caissons, especially during the most critical summer season, is negligible in these calculations. This could be because of the small volume of the caissons relative to the slide mass and to the portion of the slide mass underneath the highway (which are the slices affected by the caissons in Bishop's method); it could also be that while the gravitational driving force was reduced, so was the normal stress on the failure plane under the caissons. This would reduce the available frictional resistance to movement and counteract the reduction in driving force. Direct shear testing performed on core samples of the decomposed gneiss, through which the majority of the failure surface passes, indicates that frictional resistance contributes the majority of this material's strength, and it is therefore sensitive to changes in normal force.

Table 6. Effect of caissons on seasonal factor of safety (from Thunder, 2016).

Season	**Global Factor of Safety**	
	No Caissons	**With Caissons**
Winter	1.05	1.06
Spring	1.05	1.06
Summer	0.95	0.95
Fall	1.04	1.05

However, the caissons could have had other, unexpected effects on the slope. They are not deep enough to intersect the failure surface, but they could lend structural rigidity to the fill underneath the highway by resisting deformation. They could have influenced any settlement or consolidation that was occurring, both by creating vertical stiffness and by reducing overburden driving consolidation in the embankment below the caissons. This second effect is analogous to the removal of surcharge used for pre-consolidation of soil under future heavy structures. The soil directly underneath the caissons would have seen a 14.1% change in vertical stress, possibly sufficient to reduce consolidation rate dramatically; due to the heterogeneity and spatial variability of the embankment fill, rigorous analyses of its consolidation behavior are unfortunately not possible without more extensive field investigation.

5.3 Effects of the horizontal drains near the toe of the slide.

The horizontal drains were installed by Shannon & Wilson, Inc. in 2012, near the slide toe. Ten drains, consisting of 30.5 m (100 ft) of unslotted 3.8 cm (1.5 inch) diameter PVC pipe and another 30.5 m (100 ft) to 45.7 m (150 ft) of slotted PVC pipe, were installed in two fan-shaped groups of five drains inclined between 5° to 10° above horizontal. The approximate profile of the highest and longest drains on the slope cross-section, along with a typical profile of the peak groundwater table, is shown in Figure 18.

The limitations of the existing drain network include: the slotted section of the drain is mostly buried in the low-conductivity bedrock, and the drains are sited too low to intercept the critical buildup of pore-water pressures beneath and just upslope of the embankment. Records of drain flow rates indicate that their effect is limited; only five out of 10 drains have ever been observed producing any flow at all (Thunder, 2016), and the highest combined flow rate of these five was approximately 26.5 m^3/day (5 GPM). When distributed over the slide watershed area, this flow is equivalent to less than 0.1 mm of infiltration per day; this maximal value lasted less than a month and is two orders of magnitude less than the season-long average rate of snowmelt infiltration for that year. Drain flow rates have only been measured sporadically during site visits, so this data is incomplete.

Unfortunately, the piezometers used in this study were installed after the horizontal drains, so we do not have data available to quantitatively examine any difference the drains have made in the relationship between infiltration and groundwater levels. Thus, the approach was to estimate these differences through numerical modeling calibrating the model using flowrates measured from the horizontal drains and groundwater level observations by Kumar & Associates in 1996.

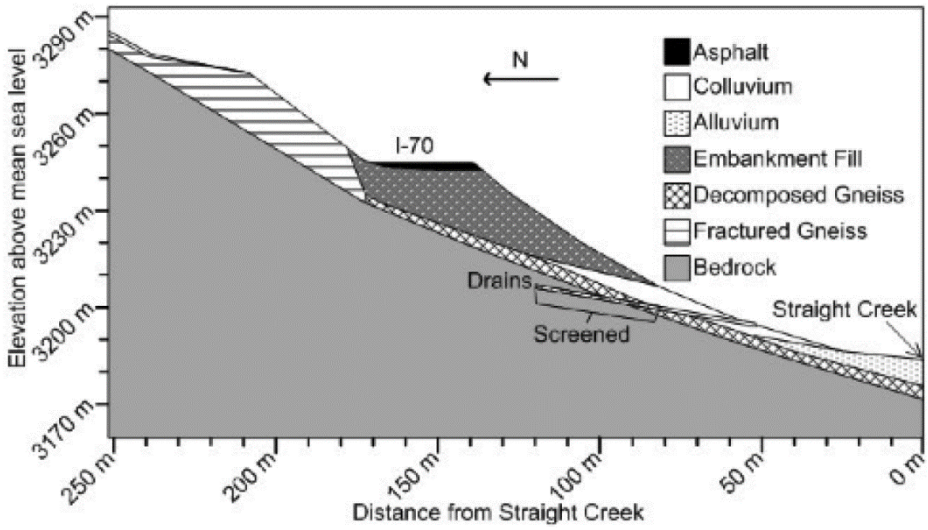

Figure 18. Position of horizontal drains (from Hinds et al., 2021).

For this purpose, the numerical model in Task II, which did not explicitly model the drains, was modified to add explicitly modeled drain elements and recalibrate the model to again match piezometer data. This was accomplished by making the following changes:

The highest and longest of the 10 installed drains is modeled to ensure that the maximum possible effect on slope stability is identified. The slotted section of the drain is modeled as a soil material with hydrologic parameters chosen to replicate drain behavior (Table 7): to draw water from the surrounding materials when they reach saturation, and to allow water to flow freely through the drain material. The thickness of this drain material layer (10 cm) is greater than the actual drainage diameter (3.8 cm); due to the large model domain, this is necessary to reduce model meshing complexity enough to allow model resolution. As the drains transect three different subsurface materials and are desired to not directly affect stability modeling, a different drain material is created for each subsurface material that the drains cross. Hydrologic parameters are the same for all drain materials, and strength parameters are set equal to the surrounding material. At the juncture of the slotted and unslotted sections of the drain-pipe, an internal opening model element is used to allow water to be removed from the model as if it were flowing through the solid section of the drain and being deposited near Straight Creek. This internal opening is assigned a “seepage face” boundary condition, which maintains a constant head of 0 m and removes any water that crosses it; this boundary condition is recommended for most drainage boundaries (Šimůnek et al., 2011). Simulated pressure heads at observation nodes corresponding to piezometer locations are

generated using daily SNOTEL infiltration data for the years over which piezometer data are available; material hydrologic properties and spatial distribution are then calibrated within ranges constrained by literature, previous laboratory testing programs, and interpretation of borehole logs to match observed piezometer data and drain fluxes as closely as possible.

Table 7. Material soil properties for numerical model that includes horizontal drains (from Hinds, et al., 2021).

Material	θ_r [-]	θ_s [-]	α [m^{-1}]	n [-]	k_s [m/day]	γ [kN/m^3]	c [kPa]	φ' [°]	E [kPa]	v [-]
Bedrock	0.06	0.34	1.374	1.72	0.001	23	5638	56	$5.3 \cdot 10^7$	0.3
Decomposed Gneiss	0.065	0.41	7.5	1.89	1.06	22	25	38	$5.0 \cdot 10^4$	0.25
Colluvium	0.08	0.33	2.35	2.12	6	20	0	34	$5.0 \cdot 10^4$	0.25
Alluvium	0.07	0.33	2.35	2.12	3	20	0	30	$5.0 \cdot 10^4$	0.25
Fractured Gneiss	0.06	0.34	1.374	1.72	40	22	1590	52	1.0×10^7	0.3
Embankment Fill	0.08	0.33	1.374	2.12	0.5	21	25	35	$3.0 \cdot 10^4$	0.25
Drain	0.07	0.5	0.5	1.65	1000	Set to match surrounding soil material				

The effect of the drains can be assessed by removing them from the calibrated model. To check that the calibration is reasonable, results of the model with no drains were compared to open well groundwater level monitoring data from Kumar & Associates (Kumar, 1997) which indicates that at their peak, groundwater levels at the eastbound and westbound shoulders may have been up to 5 m closer to each other in elevation. These bounding values are shown in Figure 19 as horizontal lines over the range of dates they were taken, with model results generated using infiltration data for the years (1996 and 1997) over which Kumar & Associates collected data for comparison. Model results are converted from pressure heads to groundwater table depth by subtracting the pressure heads from the node depth. The model used for this analysis incorporates explicitly-modeled toe drains, as discussed later in this section, so that comparing model results with Kumar & Associates observations may illustrate the effect of the drains. It is difficult to draw any definitive conclusions from this comparison. The lower groundwater position observed by Kumar & Associates under the westbound shoulder has no obvious explanation other than a systematic bias caused by instrumentation differences; the location, depth, and type of measurement all differ from the CSM piezometers. However, considering only the difference in groundwater depth

between the westbound and eastbound shoulders, the Kumar & Associates data indicates a flatter groundwater table than is both observed at the piezometers after drain installation and predicted by the model that has been calibrated to those piezometers. This could indicate that the drains have been partially successful in lowering groundwater levels downslope from the embankment, and in causing faster dissipation of elevated pore pressures beneath the eastbound shoulder and slide toe area.

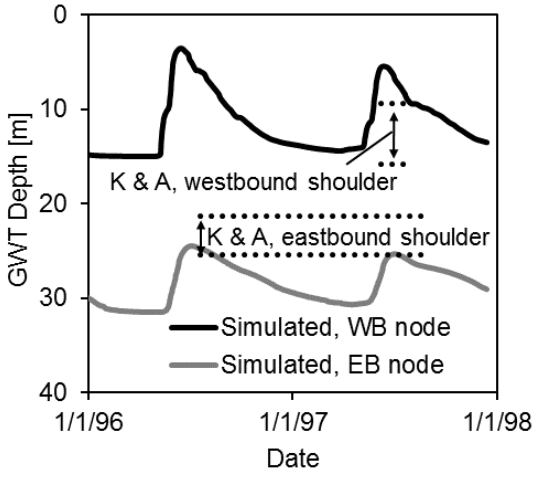

Figure 19. Groundwater table observations from Kumar & Associates, with simulated results from the same time period.(from Hinds, 2018).

Annual peak pressure heads, which are considered the most critical hydrologic result because they directly cause peak instability, generally match piezometer data very well, as do annual minimum pressure heads; the timing of pressure head change does not. Simulated groundwater elevations, calculated by adding simulated pressure head to node elevation, are compared to measured groundwater elevations on Figure 20. Simulated groundwater elevations match observed values closely at the nodes representing piezometers below the highway shoulders, where the destabilizing increase in pore-water pressure is most pronounced and critical to slope stability. Some discrepancy in the timing of pressure head changes may be explained by differences between the Straight Creek slide site and the SNOTEL station site, as explained in the previous section. This discrepancy is unlikely to affect the comparison of stability which is the purpose of this model.

In general, this model replicates peak pressure head values well; a notable exception is in 2014, when the model simulates pressure heads under the westbound and eastbound shoulder that are

substantially higher than observed pressure heads. No adjustment to material properties or distribution is able to reduce this disparity without adversely affecting model performance during other years; it seems likely that this disparity is due to differences in infiltration between the Grizzly Peak SNOTEL site, from which infiltration input data is derived, and the Straight Creek slide site. With the exception of the North node, results for minimum pressure head are also generally close to observed data. The disparity at the WB node during the winters of 2011-12 and 2012-13 are notable exceptions; given the uncharacteristically abrupt changes in piezometer data during these periods, and the fact that observed pressure heads drop to 0 m, it is possible that these are due to desaturation of the piezometer tip or other instrument malfunction.

Comparison of simulated versus measured flow from the drains requires the conversion of two-dimensional model output into a three-dimensional flux estimate. This is done by multiplying two-dimensional flows by the width of the entire drain network (150 m), so that the two- dimensional drain discharge simulated by the model can be compared to the observed collective discharge of all 10 actual drains in the drain network. The two-dimensional model represents the net effect of the discrete and distributed drain elements within the three-dimensional drain network as if they were smoothed or smeared into a constant profile.

Comparing simulated and observed flow rates poses considerable difficulties; the simulated behavior is relatively "spikier" than observed data, with no flow for most of the year and peak rates higher than any observed. The mismatch may be caused by unknown conditions within the slotted sections of the drains, such as blockages, cracks, or pinched pipes. While the peak simulated rate can be calibrated by changing drain material properties and the internal opening location or boundary condition, the temporal evolution of simulated drain outflow cannot; when the peak rate matches observed data, the simulated drain only produces flow for a few days. This results in a cumulative drain flux that is far too small. Cumulative drain flux is therefore used as the calibration measure instead of instantaneous flux because the total amount of water removed by the drains is more relevant to hydrologic behavior and slope stability than instantaneous drainage rate. However, this assumption introduces additional limitations from the scarcity of observed data; only two years, 2013 and 2015, have enough observations to approximate cumulative flow by integrating rate over time. Considerably more infiltration was experienced in 2013 than during

2015; because the simulated results reflect this and the observations do not (Figure 21), it seems likely that the flow rate measurements missed a peak in 2013, and the calculated cumulative flux is an underestimate. There is a 3.5-month gap in drain flux measurements in 2013 from mid-March to late June, which corresponds to the timing of the observed peak in 2015. Based on 2015, the one year of data that is likely to be free from substantial gaps, the model appears to adequately capture annual cumulative drain fluxes.

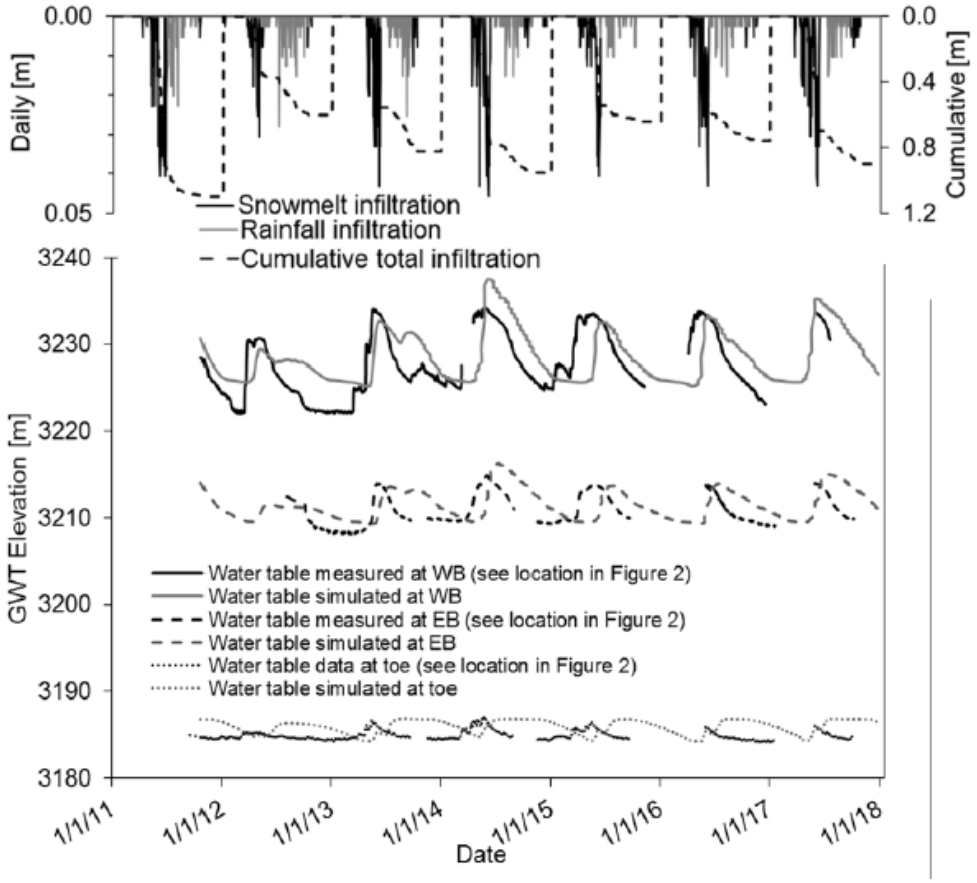

Figure 20. Comparison of simulated and measured GWT elevation (from Hinds et al., 2021).

As a final check on the reasonableness of simulated drain behavior, the Hazen-Williams (1905) formula is used to calculate the maximum flow capacity for the five active drain pipes. Using a roughness coefficient typical for PVC (150, dimensionless; Larock et al., 1940), the maximum capacity of five pipes is calculated as 1.307×10^3 m^3/day, nearly three times greater than the maximum simulated flux rate of 4.75×10^2 m^3/day and almost 50 times greater than the maximum measured flow. All simulated rates are therefore well within the range of possibility for the five active drain pipes.

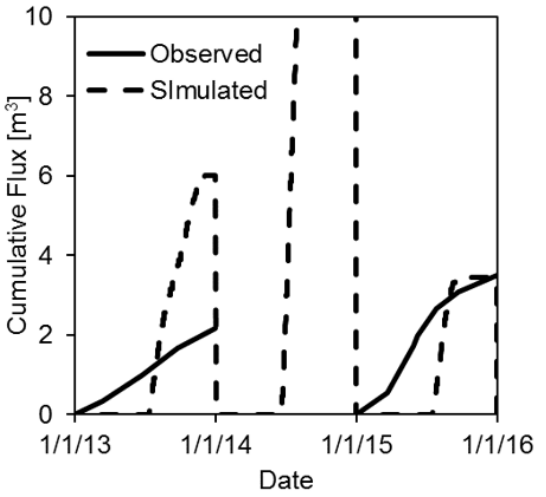

Figure 21. Observed and cumulative drain flux (from Hinds, 2018).

Once the performance of the model including explicitly-modeled drains is validated, the effect of those drains can be evaluated by removing them without changing any other part of the model. The same time period is modeled with identical infiltration inputs, so that the model without the drains simulates what the site hydrologic response during these years could have been had the drains not been installed.

The observed pressure head time series in the EB and Toe piezometers is presented in Figure 22 with the corresponding simulated pressure heads at observation nodes for the model with and without drains. Since the modeled drains have essentially no effect at all on the WB and North nodes, those results are not presented. The effect at the EB node is a slight lowering of pressure heads at all times; the difference is approximately 0.2 m. Compared to a typical peak value of about 8 m and typical winter-summer differential of 5 m, this is a small but not necessarily unimportant difference. The effect at the Toe node is more pronounced; the removal of the modeled drains increases peak pressure heads by about 0.5 m for years of average infiltration (2013, 2015 through 2017) and almost 2 m for 2011, a year of particularly high infiltration. These differences are substantial relative to a typical peak value of 4 m and typical winter-summer differential of 2.3 m. The toe drains act as a cap on pressure heads above 4 m at this node; above this level, any additional groundwater is removed by the drain. Winter-season and transitional values are also lower with the drains than without.

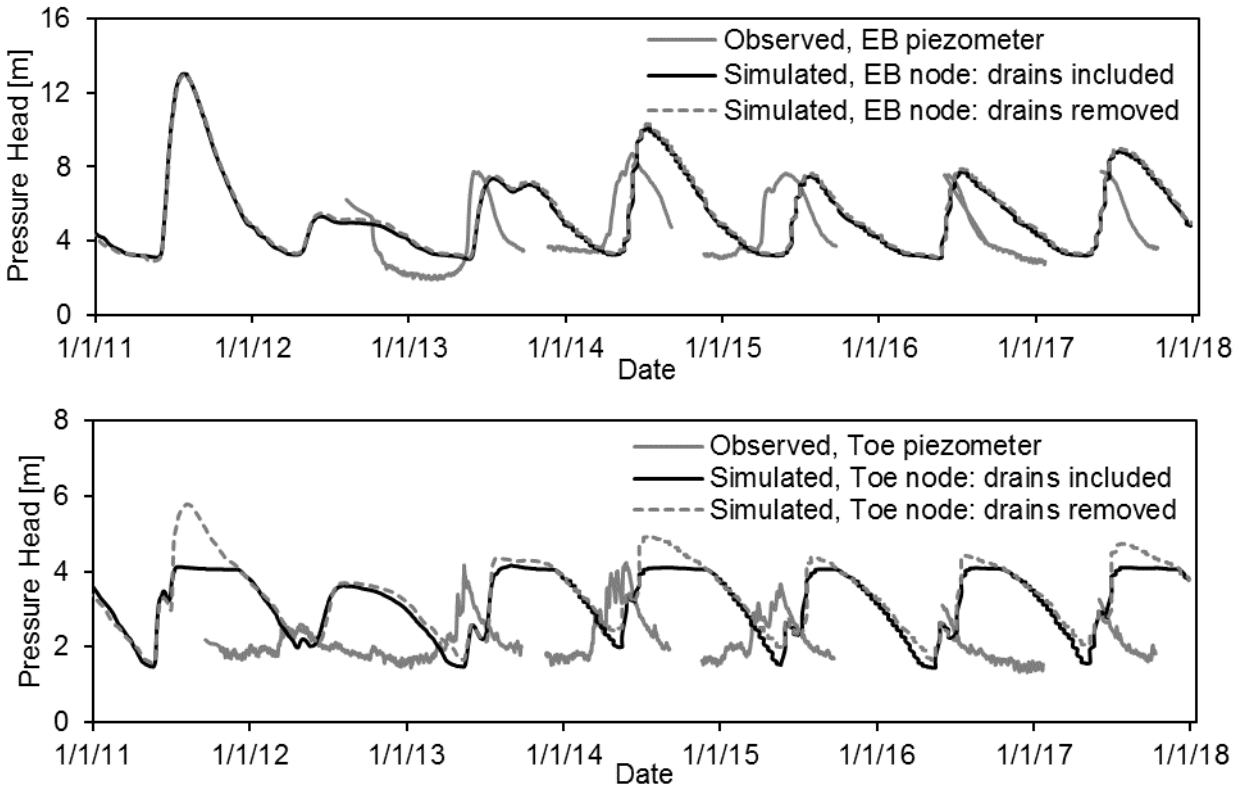

Figure 22. Observed and simulated (with and without toe drains) pressure heads at the EB and Toe nodes.(from Hinds, 2018).

Slope Cube results indicate that the drains' effect on hydrology also influences slope stability, as expected. LFS contour plots of the model with and without toe drains at the same model time step show this effect (Figure 23). This time step corresponds roughly to July 30, 2011, the least stable point in time for the modeled period (2011 through 2018, the period of piezometer data availability). The main difference is in the area directly above and below the drains, where the lower pore pressures enforced by the drains create a gap in the otherwise continuous band of LFS this point in time, although the width of the band of LFS < 1 is also reduced by the drains in the toe area. For this point in time, the difference in activated length (portion of failure surface where LFS < 1) is 2.2% of the full failure surface.

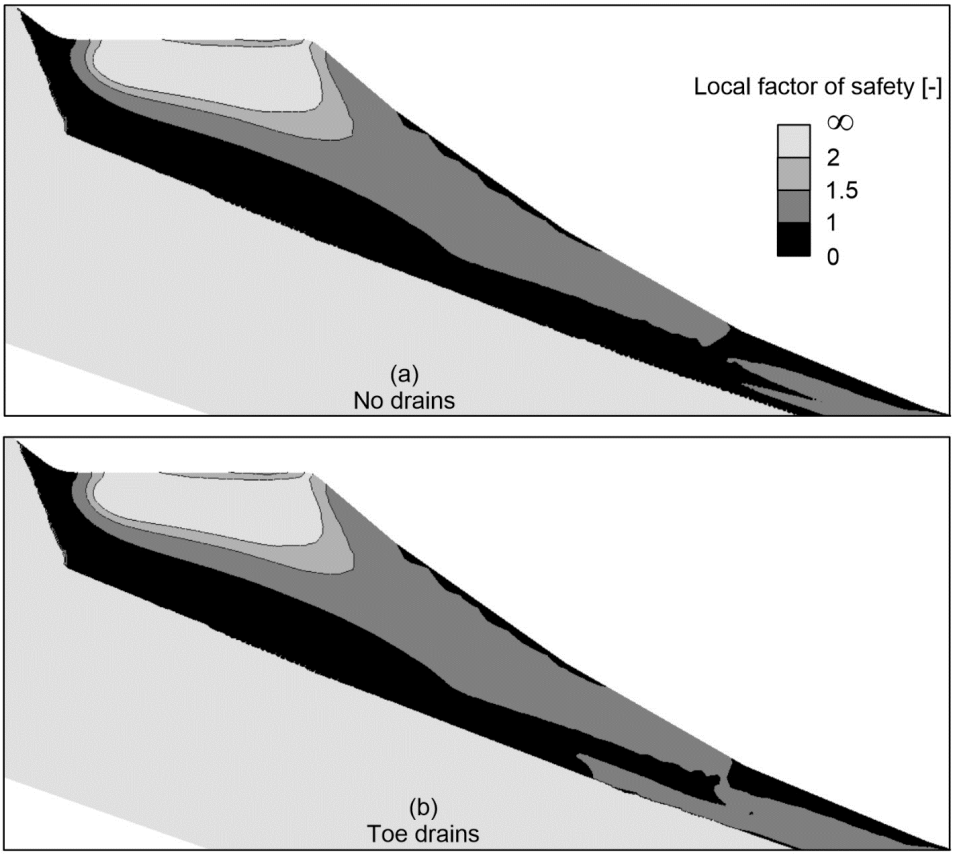

Figure 23. LFS contour plots corresponding to the least stable point in 2011 (07/30/2011) (a) without, and (b) with horizontal drains (from Hinds, 2018).

The reduction in activated length is not constant across all modeled years. To separate the effect of the toe drains from atmospheric variability, all years of available SNOTEL infiltration data are modeled with and without toe drains and the peak activated length for each year calculated (Figure 24). The effect on activated length from hydrologic variability appears to be more important than the effect of the toe drains. The difference in activated length for a year of maximal annual cumulative infiltration (2011) versus a year of minimal annual cumulative infiltration (2012) is 61.1% of the full failure surface, whereas the greatest reduction in activated length caused by the toe drains is 14.2% of the full failure surface (1999). The average difference in activated length caused by the toe drains is 2.7% of the full failure surface, and the effect is negligible for years of maximal annual cumulative infiltration (e.g., 0.01% of the full failure surface in 2011, and 0.75% of the full failure surface in 1996). The combination of hydrologic variability and the toe drains may be sufficient to explain the lack of substantial movement since 2012. Only one year (2014) in the period following installation of the toe drains has a peak activated length above 62.5% (identified as a critical stability threshold for the Straight Creek slide during model calibration)

when modeled with the toe drains, and that peak activated length is only 4.4% above this threshold. If the model is slightly underestimating the drains' effect on embankment stability, the combination of toe drains and hydrologic variability could explain the reduced movement rate.

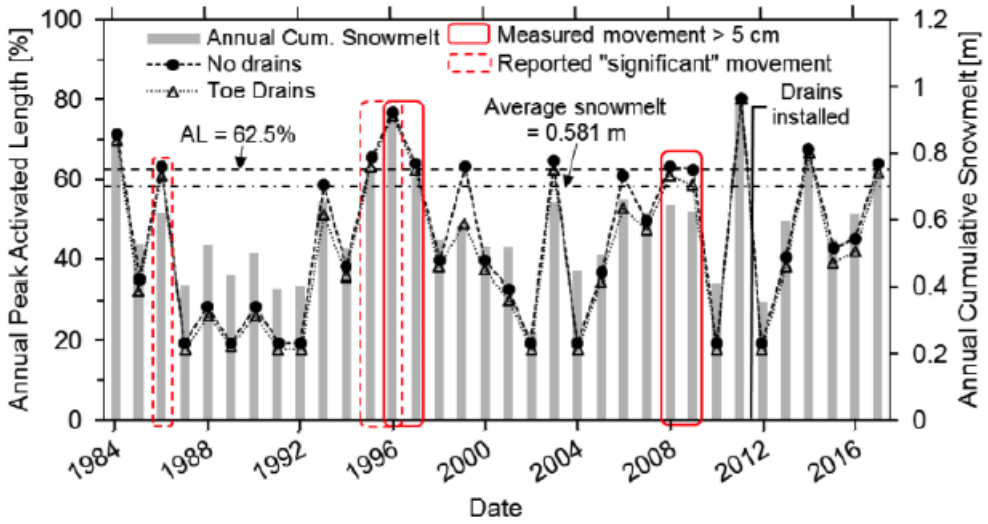

Figure 24. Annual peak activated length for different years, for cases with and without horizontal drains near the toe (from Hinds et al., 2021).

The reduction in movement since 2012 is also possibly due to the slide mass having reached a temporarily metastable position or configuration. Based on their survey monument data, Kumar & Associates (Kumar, 1997) hypothesized that slide movement occurred in cycles over several years, with movement initiating at the eastern boundary and progressing westward. This suggests a buildup of shear stress along the failure surface due to internal movements of the slide mass, which is released progressively across the slide zone. The current period of reduced movement could correspond to a quiescent phase during which shear stress is increasing; this stored shear stress could be released as slide movement, either by reaching a critical point or by being triggered by a year of elevated cumulative infiltration. Particularly destabilizing infiltration characteristics (above average annual cumulative snowmelt infiltration occurring at a higher-than-average rate; Hinds et al., 2019), such as occurred in 1984, 1996, and 2011, can still produce an activated length well above the 62.5% threshold even with the toe drains included in the model. Thus, the embankment may experience substantial movement within the next decade if the historical frequency of above average snow accumulation is repeated in the future.

A conventional global factor of safety analysis using Bishop's modified method of slices also indicates a modest improvement in stability from the toe drains. Groundwater positions for the least stable points in 2011 (July 30) and 2013 (August 30), obtained from the numerical model, are used for pore pressure calculations, and a uniform suction stress of -5 kPa (based on model results) is assumed for segments of the failure surface above the groundwater table (Figure 25). Without toe drains, this analysis calculates a global FS of 0.96 for 2011 and 1.13 for 2013; with toe drains, the FS improves to 0.97 and 1.16, respectively. Again, for a year that is just unstable enough to see substantial movement, the toe drains may be effective enough to increase stability; however, for a year of particularly high instability these drains most likely will not be effective in preventing movement.

There remains great deal of uncertainty about the degree of the toe drains' effect, mostly due to the uncertainty about how much water they are actually removing from the slide site. More-frequent collection of drain flow rates may help resolve this uncertainty.

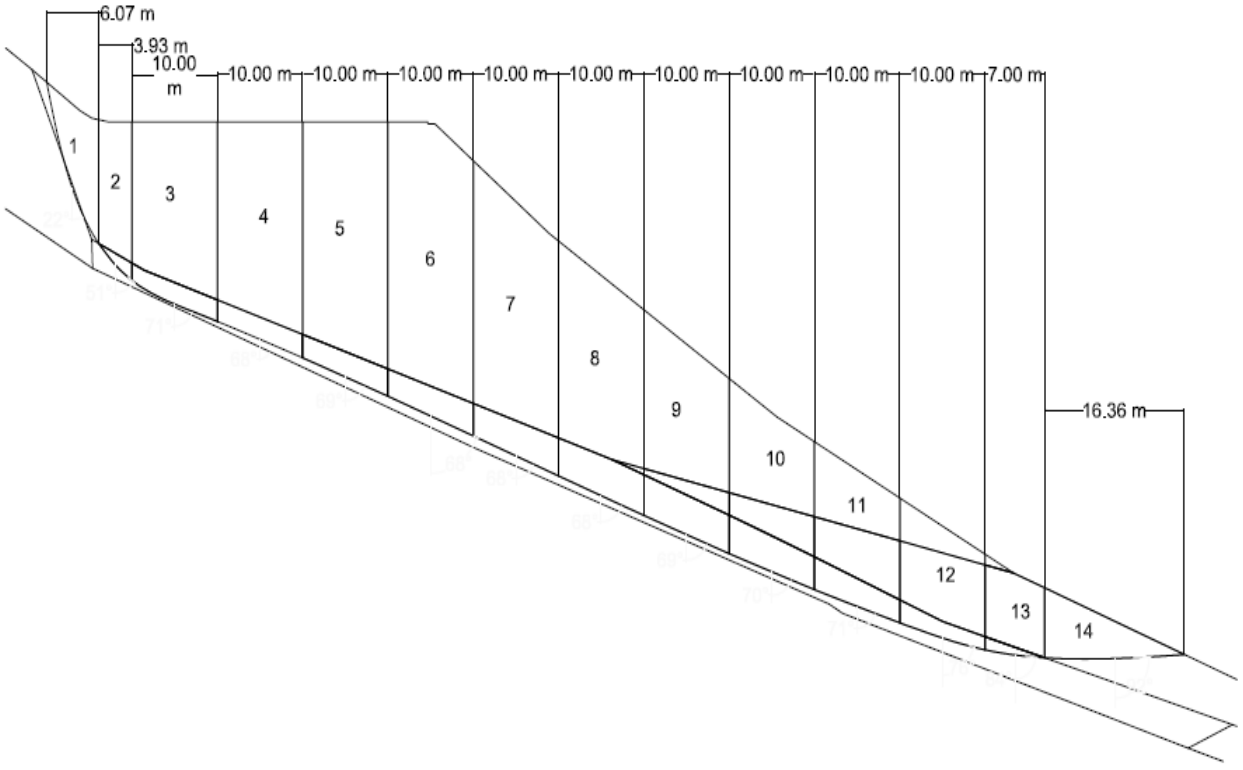

Figure 25. Slide geometry for method of slices analysis (from Hinds, 2018).

6. TASK IV: EVALUATION OF DRAIN SYSTEM NORTH OF I-70

While the existing toe drains had a modest effect improving the site drainage and stability, the insights gained through the three phases of this investigation indicate that a remediation approach targeting the primary driver of slope movement could have a greater impact. The hydrology of the Straight Creek slide creates a very specific failure mechanism, which can be specifically addressed to maximize the impact of remediation work. Based on modeling results, the main cause of this slide is the infiltration of snowmelt on the northern slope above the highway, which flows rapidly downslope until it hits the sharp contrast in hydraulic conductivity created by the decomposed gneiss and embankment material. The resulting spike in pore pressures directly causes the seasonal loss of stability that has led to recurring slide movement over the majority of the embankment's service life. If the backup of groundwater is prevented from happening in the first place, the slide could be stabilized more effectively.

One feasible approach to achieve this is to install a drain system in the north slope, above the westbound shoulder of I-70 (Figure 26). A limiting factor on the location of the toe drain system was drill rig access; installing the drains any higher up would have required getting a rig up the increasingly steep, topographically rugged slope, which is covered in loose talus and colluvium and closely spaced trees. Drains extending into the north slope could be drilled from the 11 m wide, flat, paved westbound shoulder, with easy access for machinery, supplies, and personnel.

The preliminary design considered here consists of 12 drains in four fanned groups of three, spaced at even intervals of about 50 m along the side of I-70, projecting perpendicularly from the westbound shoulder of the highway at a pitch of 10°. The drains would consist of similar PVC pipe as the toe drains, extending the same distance (70 m) past the surface. Modeling of these drains suggests that a longer slotted section is desirable, with only the final 15 m consisting of solid pipe; this would allow for as much water to be removed from the shallow subsurface as possible. The drains would empty into a culvert running parallel to the westbound shoulder to carry water downslope to the lined Harrison Gulch culvert approximately 680 m to the west, which already runs underneath the highway towards Straight Creek.

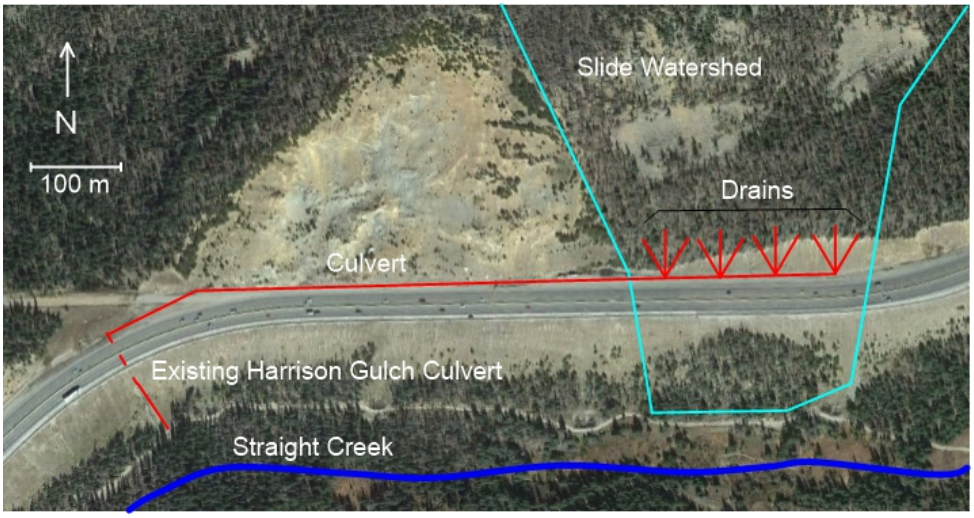

Figure 26. Plan of proposed north slope drain system; drain elements are shown in red, Straight Creek in blue, and approximate slide site watershed extents in cyan (from Hinds, 2018).

6.1 Numerical modeling of new drain system

To assess the potential effect of the proposed mitigation strategy, a similar drain modeling approach is used. Instead of ending in an internal opening with a seepage face boundary, the drain material is extended all the way to the surface and assigned a constant head boundary of -3 m. This boundary condition is designed to replicate field conditions by allowing water in the drain material to be removed from the model; while it is not physically consistent, it is a necessary workaround for adapting a numerical modeling software package to a problem it was not designed to solve. Unlike the internal opening where the toe drain material terminates, the area where the north slope drain material terminates does not become saturated under any modeled conditions; if a seepage face boundary condition is used, the water in the drain material flows to the surface but cannot be removed as it does not reach a pressure head of 0 m. Before that point is reached the water flows out of the drain material into the embankment material, so that the north slope drains increase pore water pressures underneath the embankment by transporting water rapidly from deep in the north slope and then releasing it back into the subsurface right above the embankment. Figure 27 shows the geometry of Phase III modeling of the north slope drains.

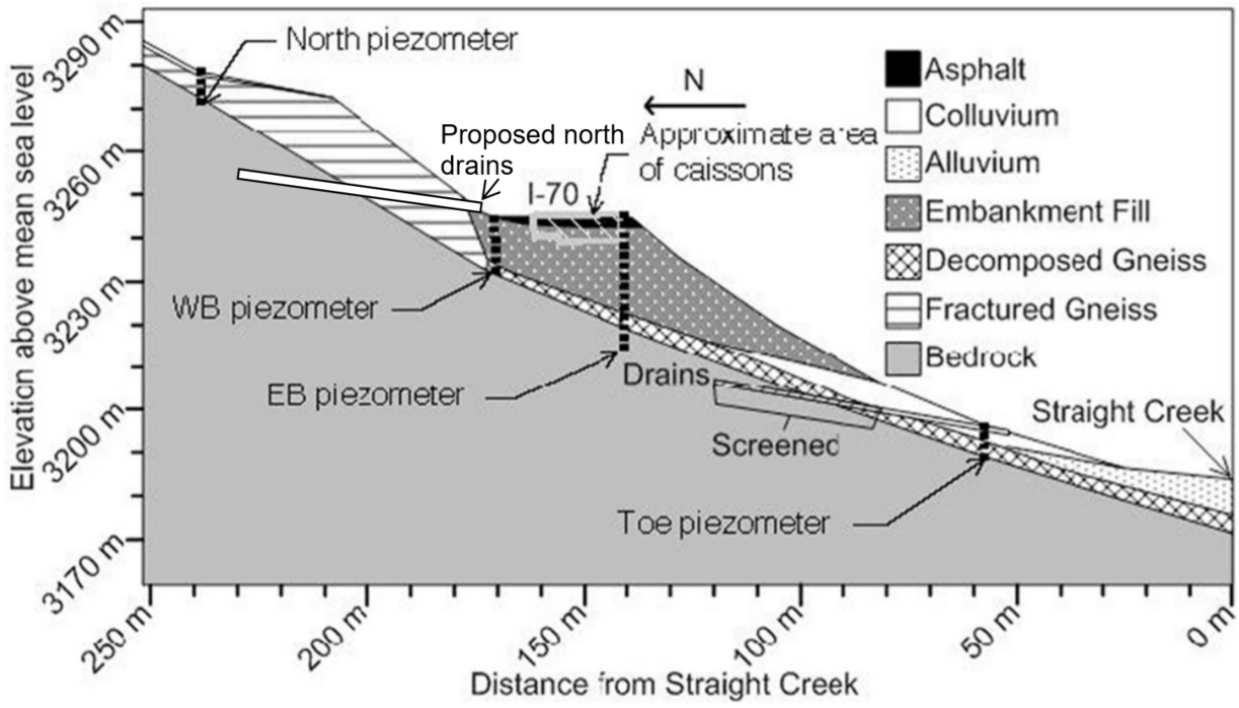

Figure 27. Numerical model geometry that integrates north slope drains (modified from Hinds et al.,2021.

6.2 Evaluation of drain network North of I-70

The effect of this hypothetical drain system on pressure heads at the observation nodes is shown in Figure 28, with the observed piezometer data and simulated pressure heads from the Phase III model with and without toe drains for comparison. These drains affect peak pressure heads, which are lowered by about 0.75 m at the North node, 5 m at the WB node, 4 m at the EB node, and 2 m at the Toe node. The WB node is the most strongly affected, as it is the closest to the north slope drains. Pressure head peaks at this node are reduced the most, and their shape is also substantially affected; elevated pore pressures dissipate faster. In 2011, which had the second-highest cumulative infiltration of any year since 1984, pressure head at the WB node does still increase notably (peak value 14 m, versus 20 m without the north slope drains); this seems to indicate that the extremely high infiltration is exceeding the capacity of the drain material. However, the highest simulated flux from the north slope drain boundary is only 650 m^3/day, which is well below the full-pipe capacity of 10 drains as calculated earlier; the performance of the north slope drains may in fact be underestimated by the model.

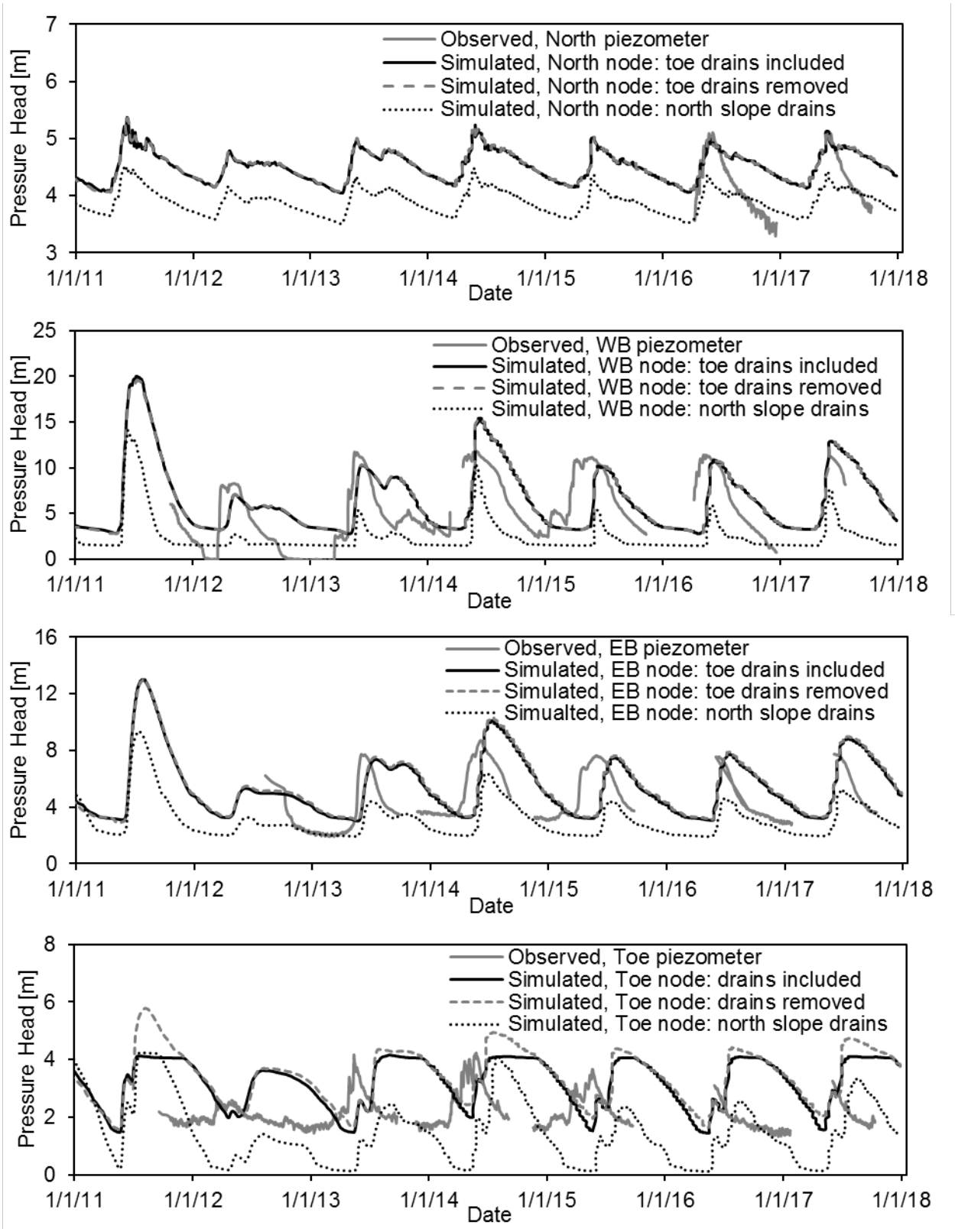

Figure 28. Observed and simulated pressure heads at the observation nodes, for models with and without toe drains and north slope drains (from Hinds, 2018).

The effect of the proposed drains in pore-water pressures has a significant impact on the hillslope stability. Local factor of safety contour plots for the model with only toe drains and the model with toe drains and north slope drains indicate a greatly reduced region of LFS < 1 beneath the embankment (Figure 29).

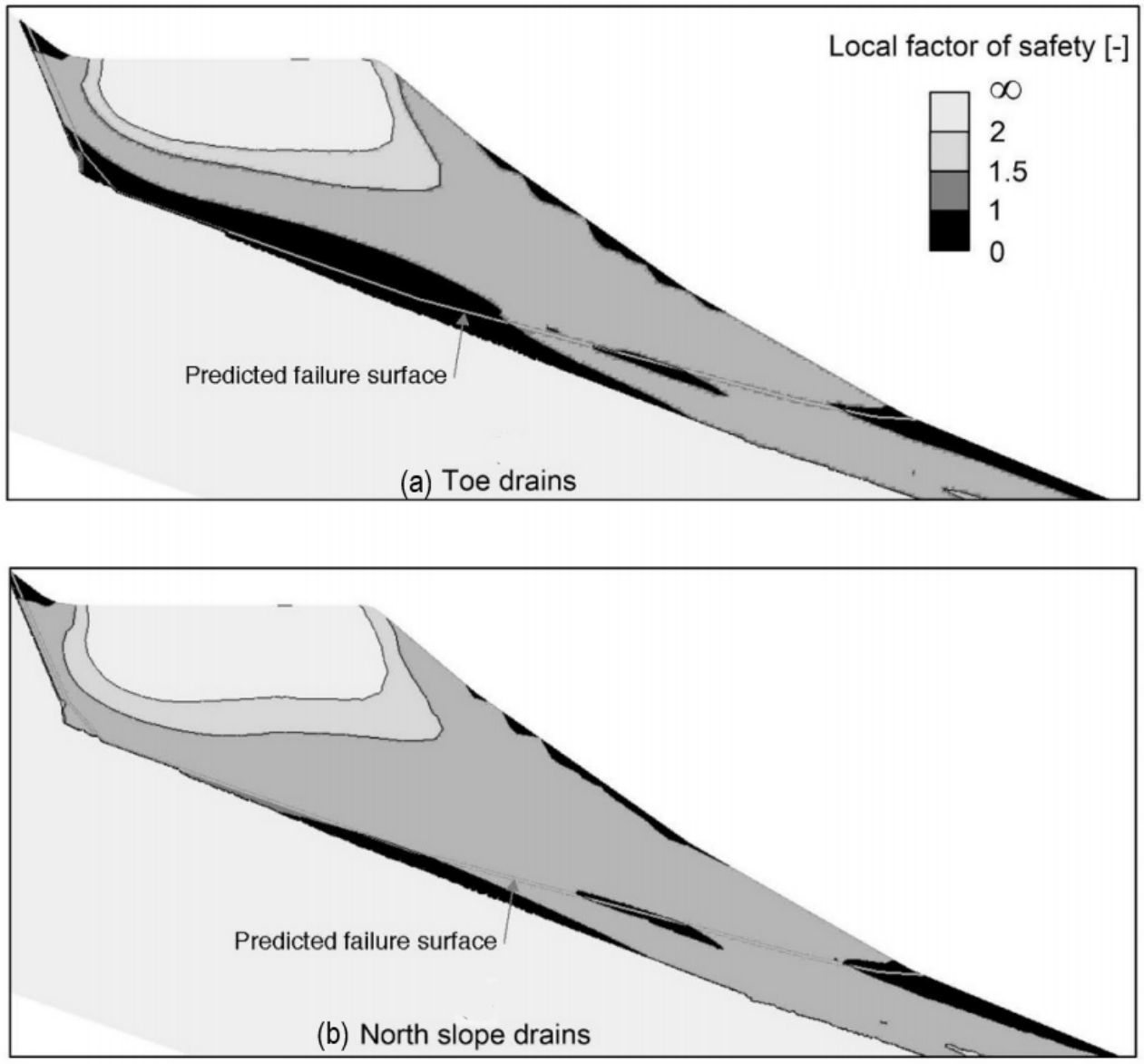

Figure 29. LFS contours at from a time step corresponding to the least stable point in 2011, for the model (a) with only toe drains and (b) with both toe drains and north slope drains.

When modeled with the north slope drains, only 4 of the 34 years of available infiltration data show any increase in activated length over minimal, wintertime values (15.3% of the full failure

surface). Annual peak activated lengths calculated over the period of available infiltration data illustrate that the effect of the north slope drains could result in a substantial improvement in stability (Figure 30). No year modeled with the north slope drains has a peak activated length above the 62.5% threshold, which was the lowest peak activated length for a year of known increased movement. Only 2011, the year of highest annual cumulative infiltration, has an activated length above 40% of the full failure surface. The toe drains reduce peak activated length by an average value of 2.7% of the full failure surface when compared to the model without any drains; the north slope drains reduce peak activated length by an average value of 24.8% of the full failure surface when compared to the toe drains, a more substantial improvement in predicted stability.

Conventional global FS analyses using Bishop's modified method of slices also indicate that the north slope drains could be more effective than past remediation techniques. Groundwater positions for the least stable points in 2011 (July 21) and 2013 (July 10), derived from model results, are used for pore-water pressure calculations, and a uniform suction stress of -5 kPa is assumed for segments of the failure surface above the groundwater table. For the least stable point in 2011, the global FS without any drains is 11% smaller than the FS with north slope drains, and in 2013, the FS without drains is 8.6% smaller than the FS with north slope drains. Thus, the north slope drains are more effective in eliminating progressive failure and small slide movements in years of average infiltration.

The proposed north slope drains network is just one possible effective remediation. They have the potential to substantially change the stability of the Straight Creek slide, possibly eliminating slide movement altogether. They could accomplish this for a smaller cost than has already been spent on remediation for this site, eliminate the expenditure on annual asphalt capping operations that are currently necessary to maintain roadway serviceability, and not require any traffic lane closures. We conclude that a Phase IV study to engineer an optimum upslope drain system would result in a long-term solution to the Straight Creek slide problem.

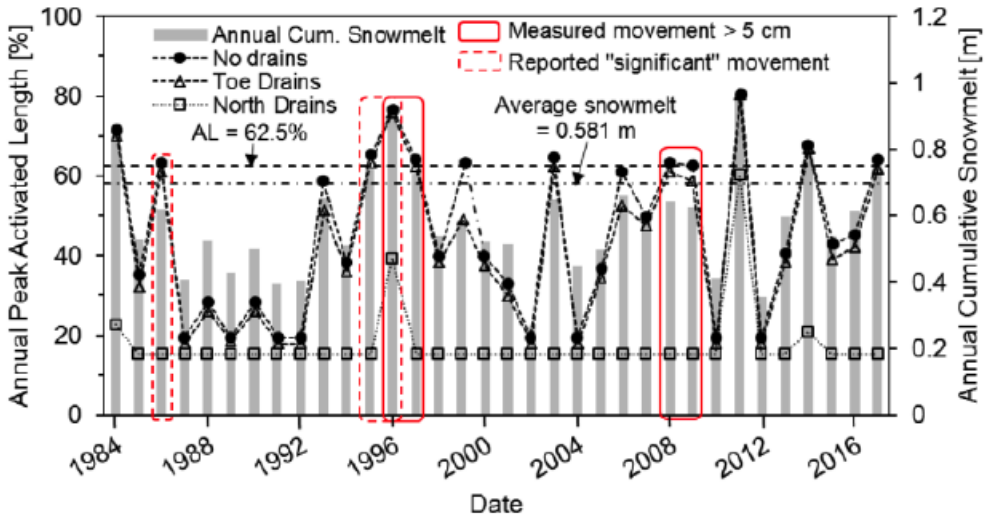

Figure 30. Annual peak activated length for no drains (circles), toe drains (triangles), and North drains (squares) (from Hinds et al., 2021).

7. SUMMARY AND CONCLUSIONS

Infiltration-induced landslides are a dangerous geological hazard in the United States, and their occurrences result in expensive damages that often claim lives. Many of these landslides are triggered by a change in the hydrological conditions at the site. In 2010, a three-phase joined effort between Colorado School of Mines, CDOT, and the Landslides Hazards Program of the United States Geological Survey was setup to implement a novel approach that integrates field monitoring observations, laboratory testing, and a hydro-mechanical framework in the analysis and prediction of landslides. The site identified for this study is the Straight Creek landslide, west of the Eisenhower/Johnson Memorial Tunnels. This document reports the findings of the third phase of this investigation which includes field monitoring, an analysis of the slope stability sensitivity to single year and multiyear variable infiltration, evaluation of two mitigation techniques implemented at the site, and recommendations for a preliminary site remediation solution.

The analyses in this report were based on data obtained from eight piezometers, five inclinometers, one stream gage, a SNOTEL station, and anecdotal reports both oral and documented in previous studies. Consistent to observations in Phase II of this study, groundwater level underneath the westbound shoulder changes twice as much as groundwater level underneath the eastbound shoulder. This confirms that infiltration of snowmelt on the northern slope above the highway is significant and that paired with the sharp contrast in hydraulic conductivity underneath the highway, produces

a peak in pore water pressures and affects the stability of the hillslope. Based on older and newer inclinometer readings, field observations, and numerical analysis results, the failure plane of the landslide is believed to start near the westbound shoulder of I-70 and run along the decomposed gneiss-bedrock interface.

From the spatiotemporal evolution analysis of slope failure due to changes in the hydrology of the hillslope, the following conclusions are drawn:

- Instability at this site is directly triggered by an abrupt dramatic seasonal increase in pore pressure beneath the embankment, which is caused by the rapid infiltration of snowmelt.
- Slope stability is sensitive to annual cumulative snowmelt infiltration and rate at which snowmelt occurs. Of the infiltration characteristics studied, annual cumulative snowmelt infiltration is by far the most important single-year factor in the level of slide activation and is likely sufficient to determine whether the slide will move and by how much in a given year. The rate at which snowmelt occurs also has a substantial effect on stability, although less so than the total amount of snowmelt. A faster rate of snowmelt exacerbates the seasonal increase in pressure head beneath the embankment, which is the cause for instability.
- Slope stability can be affected by infiltration in the previous year. Consecutive years of high infiltration can have a compounding effect, increasing the magnitude of seasonal pressure head rise and resulting in less stability than single, isolated years of high infiltration. Likewise, consecutive years of low infiltration can suppress groundwater response to infiltration and increase slope stability in subsequent years.
- Smaller movements in the last five years may be explained by the combination of cumulative snowmelt infiltration, snowmelt infiltration rate, and infiltration in previous years.

From the evaluation of the effect of lightweight caissons and horizontal drains installed at the site in 2011 and 2012, the following conclusions can be drawn:

- The use of lightweight caissons to reduce the slide mass was minimally effective. The caissons reduced weight of the slide mass by 0.9%, which translated in a change in FOS of less than 1%. Remediation techniques that address the pore water pressure are more effective.
- The installation of horizontal drains near the slide toe had a modest effect on site stability. Pore pressures are only reduced in a localized area near the drains, but due to the low hydraulic conductivity of the embankment materials, it is ineffective beneath the embankment.
- The drains may have been sufficient to stabilize the embankment during the period of low to average annual cumulative infiltration, but not for years of higher annual cumulative infiltration.

Based on the results of this study, the main cause of this slide is the infiltration of snowmelt on the northern slope above the highway, which flows rapidly downslope until it hits the sharp contrast in hydraulic conductivity created by the decomposed gneiss and embankment material. Thus, we conclude that a remediation solution could be engineered to prevent large increases in pore water pressures north of I-70. One preliminary design is a 12 horizontal drains network north of I-70; for such a system, the numerical analysis indicates:

- The seasonal reduction of stability at the Straight Creek slide is eliminated, even for years of higher annual cumulative infiltration. This is a significant improvement compared to the minimal effect on factor of safety of the installation of lightweight caissons.
- A critical threshold for slide movement under conditions similar to years 1984-2018 is not crossed.
- The proposed drains intercept upslope flow before the hydraulic conductivity contrast at the embankment; therefore, the intercepted flow could be safely diverted away from the embankment.
- The proposed remediation has easier access for equipment and personnel.

8. FURTHER ACTIONS

Based on all the data obtained from previous reports and during the past three phases of this study, it is clear that the main cause of this slide is the infiltration of snowmelt on the northern slope above the highway. This large infiltration through decomposed gneiss, paired with a sharp contrast in hydraulic conductivity of materials underneath the highway, results in an increase of pore water pressures and a decrease in the stability of the slope. Thus, we conclude that a remediation solution could be engineered to prevent large increases in pore water pressures north of I-70. The analyzed preliminary design for a drainage system provides encouraging results. A Phase IV: Study and Engineer of Optimum Upslope Drain System would be needed to adequately optimize the long-term solution of the study site. This new study could include:

- Numerical analyses of other drain configurations to find the most effective alternative.
- Installation of proposed drain system.
- Monitoring of drain system, groundwater table, and stability of hillslope.

9. REFERENCES

Bogaard, T. and Greco, R. (2018). "Invited perspectives: A hydrological look to precipitation intensity duration thresholds for landslide initiation: Proposing hydro-meteorological thresholds." *Natural Hazards and Earth System Science*, 18(1): 31–39. https://doi.org/10.5194/nhess-18-31-2018

Campbell, R. H. (1975). "Soil slip, debris flows, and rainstorms in the Santa Monica Mountains and vicinity, southern California." *U.S. Geological Survey Professional Paper 851*, 58 pp. https://doi.org/10.3133/pp851

Chleborad, A. F. (1998). "Use of air temperature to anticipate the onset of snowmelt season landslides." *U.S. Geological Survey Open File Report 98-124*, 17 pp. https://doi.org/10.3133/ofr98124

Hinds, E. (2018). *Effects of atmospheric variability and remediation techniques on the stability of an interstate highway embankment*. M.S. Thesis, Colorado School of Mines: Golden, CO, 167 pp. https://hdl.handle.net/11124/172344

Hinds, E., Lu, N., Mirus, B., Wayllace, A. (2019). "Effects of Infiltration Characteristics on Spatial-Temporal Evolution of Stability of an Interstate Highway Embankment." *Journal of Geotechnical and Geoenvironmental Engineering*, 145(9): 05019008. https://doi.org/10.1061/(ASCE)GT.1943-5606.0002127

Hinds, E. S., Lu, N., Mirus, B. B., Godt, J. W., & Wayllace, A. (2021). Evaluation of techniques for mitigating snowmelt infiltration-induced landsliding in a highway embankment. *Engineering Geology*, 106240.

Kumar & Associates. (1997). Progress report of geological and geotechnical data acquisition, embankment slope instability study, Straight Creek, Interstate-70 west of Eisenhower Tunnel, Summit County, Colorado.

Lim, K., Engel, B., Tang, Z., Choi, J., Kim, K., Muthukrishnan, S., and Tripathy, D. (2005). "Automated web GIS based hydrograph tool, WHAT." *Journal of the American Water Resources Association*, 41(6): 1407–1416. https://doi.org/10.1111/j.1752-1688.2005.tb03808.x

Lu, N., and LeCain, G. (2003). “Percolation induced heat transfer in deep unsaturated zones.” *Journal of Geotechnical and Geoenvironmental Engineering*, 129(11): 1040–1053. https://doi.org/10.1061/(ASCE)1090-0241(2003)129:11(1040)

Lu, N., and Likos, W.J. (2004). *Unsaturated Soil Mechanics,* John Wiley and Sons.

Lu, N., and Likos, W. J. (2006). "Suction stress characteristic curve for unsaturated soils," *Journal of Geotechnical and Geoenvironmental Engineering,* Vol. 132(2), 131–142.

Lu, N., (2008). “Is matric suction a stress variable?” *Journal of Geotechnical and Geoenvironmental Engineering*, Vol. 134(7), 899-905.

Lu, N., & Godt, J. W. (2013). *Hillslope hydrology and stability*. Cambridge University Press.

Lu, N., Godt, J. W., and Wu, D. T. (2010). ″A closed‐form equation for effective stress in unsaturated soil,″ *Water Resources Research*, Vol. 46(5).

Lu, N., Wayllace, A., and Oh, S. (2013). “Infiltration-induced seasonally reactivated instability of a highway embankment near the Eisenhower Tunnel, Colorado, USA.” *Engineering Geology*, 162: 22–32. https://doi.org/10.1016/j.enggeo.2013.05.002

Lu, N., Wayllace, A., and Formetta, G. (2016). *The Slope Cube Module for HYDRUS (2D): Simulating Slope Stress and Stability in Variably-Saturated Hillslopes*, Technical Manual, Version 1.0, Soil Water Retention LLC.

Mirus, B. B., Becker, R. E., Baum, R. L., and Smith, J. B. (2018a). “Integrating real-time subsurface hydrologic monitoring with empirical rainfall thresholds to improve landslide early warning.” *Landslides*, 15(10): 1909–1919. https://doi.org/10.1007/s10346-018-0995-z

Mirus, B. B., Morphew, M. D., and Smith, J. B. (2018b). “Developing hydro-meteorological thresholds for shallow landslide initiation and early warning.” *Water*, 10(9): 1274. https://doi.org/10.3390/w10091274

Mualem, Y. (1976). "A new model for predicting the hydraulic conductivity of unsaturated porous media," *Water Resources Research*, 12(3), 513-522.

Nathan, R. and McMahon, T. (1990). "Evaluation of automated techniques for base flow and recession analyses." *Water Resources Research*, 26(7): 1465–1473. https://doi.org/10.1029/WR026i007p01465

NRCS (2018). "Colorado SNOTEL Site Number 505 Grizzly Peak." *United States Department of Agriculture, Natural Resources Conservation Service.* https://wcc.sc.egov.usda.gov/nwcc/site?sitenum=505

Richards, L. (1931). "Capillary conduction of liquids through porous mediums," *Journal of Applied Physics*, Vol. 316.

Šimůnek, J., van Genuchten, M. Th., and Šejna, M. (2011). *The HYDRUS Software Package for Simulating Two- and Three-Dimensional Movement of Water, Heat, and Multiple Solutes in Variably-Saturated Media*, Technical Manual, Version 2.0, PC Progress SRO.

Thomas, M. A., Mirus, B. B., Collins, B. D., Lu, N., and Godt, J. W. (2018). Variability in soil-water retention properties and implications for physics-based simulation of landslide early warning criteria: *Landslides*. https://doi.org/10.1007/s10346-018-0950-z

Thunder, B. (2016). *The Hydro-mechanical Analysis of an Infiltration-Induced Landslide Along I-70 in Summit County, CO*. Master's Thesis, Colorado School of Mines: Golden, CO, 83 pp. http://hdl.handle.net/11124/170303

USGS (2018). "USGS Stream Gage 09051050: Straight Creek below Laskey Gulch near Dillon, CO." *U.S. Geological Survey, National Water Information System*. https://waterdata.usgs.gov/monitoring-location/09051050/

USGS StreamStats (2018). "StreamStats: Streamflow Statistics and Spatial Analysis Tools for Water-Resources Applications, Version 4.2.0." U.S. Geological Survey, Web Informatics and Mapping Team. https://streamstats.usgs.gov/

van Genuchten, M. Th. (1980). "A closed form equation for predicting the hydraulic conductivity of unsaturated soils," *Soil Science Society of American Journal*, Vol. 44, 892-898.

Wayllace, A., Lu, N., Oh, S., and Thomas, D. (2012). "Perennial infiltration-induced instability of Interstate-70 embankment west of the Eisenhower/Johnson Memorial Tunnels." In Hryciw, R. D., Athanasopoulos-Zekkos, A., and Yesiller, N. (eds.) *GeoCongress 2012: State of the Art and Practice in Geotechnical Engineering*, Geotechnical Special Publication 225: 497–506. https://doi.org/10.1061/9780784412121.052

Wayllace, A. and Lu, N. (2011). "A Transient Water Release and Imbibitions Method for Rapidly Measuring Wetting and Drying Soil Water Retention and Hydraulic Conductivity Functions." *Geotechnical Testing Journal*, 35(1): 103–117. https://doi.org/10.1520/GTJ103596

Wayllace, A., Lu, N., Godt, J. (2017). "In-situ monitoring of infiltration-induced instability of I-70 embankment west of the Eisenhower-Johnson Memorial Tunnels, Phase II." (Report No. CDOT-2017-12). Colorado Department of Transportation. https://www.codot.gov/programs/research/pdfs/2017-research-reports/insitu-phase-2

Wayllace, A. Thunder, B., Lu, N., Khan, A., and Godt, J. W. (2019). "Hydrological Behavior of an Infiltration-Induced Landslide in Colorado, USA." *Geofluids*, 2019: 1959303. https://doi.org/10.1155/2019/1659303

Whipkey, R. Z. (1969). "Storm runoff from forested catchments by subsurface routes." *Proceedings of the International Association of Hydrological Sciences*, 85: 773-779. https://iahs.info/uploads/dms/17979.08522.pdf

Wieczorek, G. F. and Glade, T. (2005). "Climatic factors influencing occurrence of debris flows." In Jakob, M. and Hungr, O. (eds.) *Debris-flow hazards and related phenomena*, Springer-Praxis: Berlin, 325–362. https://doi.org/10.1007/3-540-27129-5_14

APPENDIX A
CSM BOREHOLE LOGS

BORING LOG 08/31/2011 BOREHOLE 1 - WESTBOUND I-70 SHOULDER AT MM 212,
Drilled: CDOT (D. Novak) 166 FT WEST OF ELECTRICAL BOX
Logged: CSM, USGS (M. Morse, A. Wayllace)

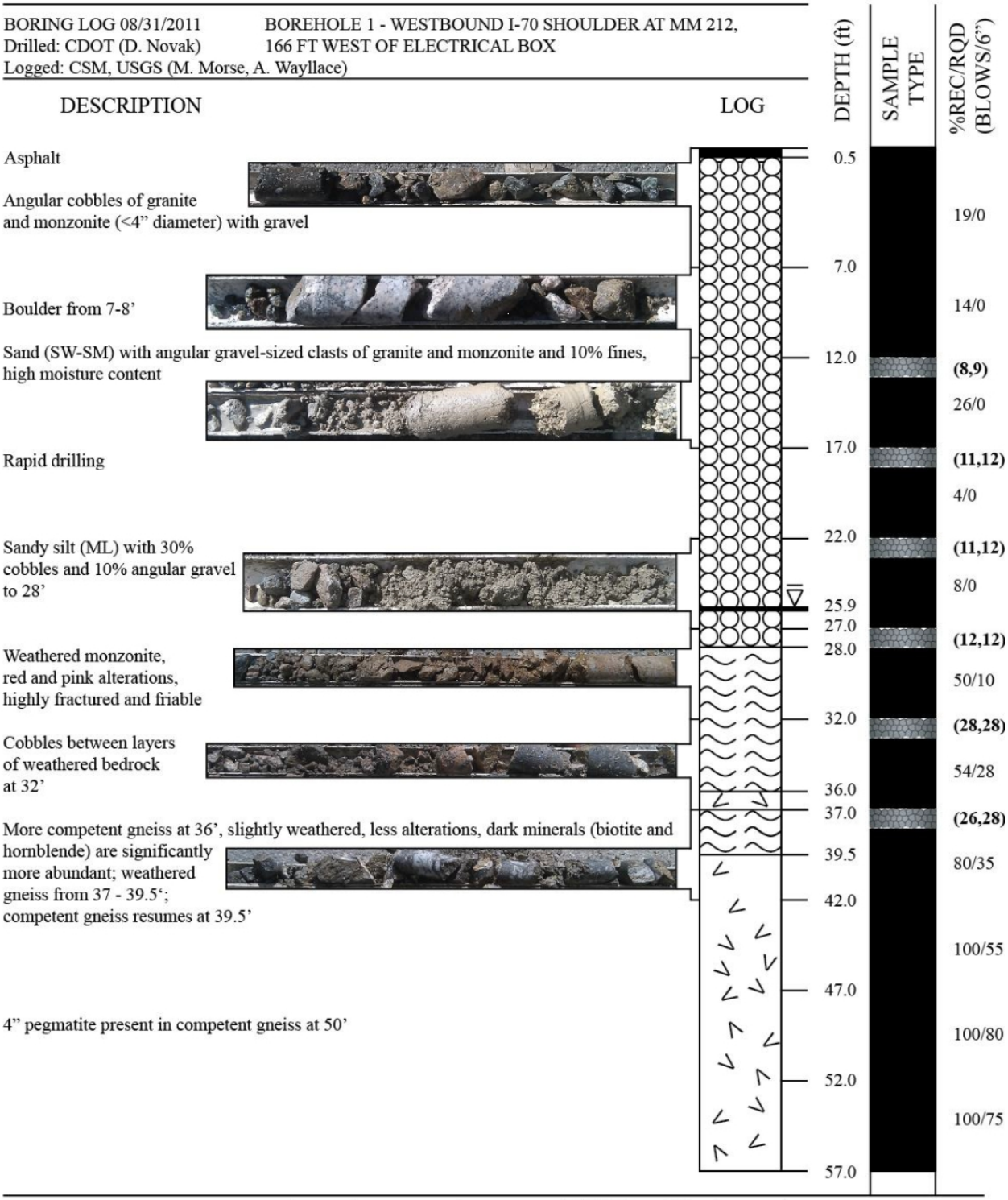

LEGEND

- Cobbles with sandy or silty matrix
- Core sample
- Highly weathered gneiss
- California sample
- More competent gneiss; bedrock

BORING LOG 09/15/2011 BOREHOLE 2 - 300' DOWNSLOPE FROM I-70 EASTBOUND
Drilled: CDOT (D. Novak) GUARD RAIL, MM 212
Logged: CSM, USGS (M. Morse, A. Wayllace)

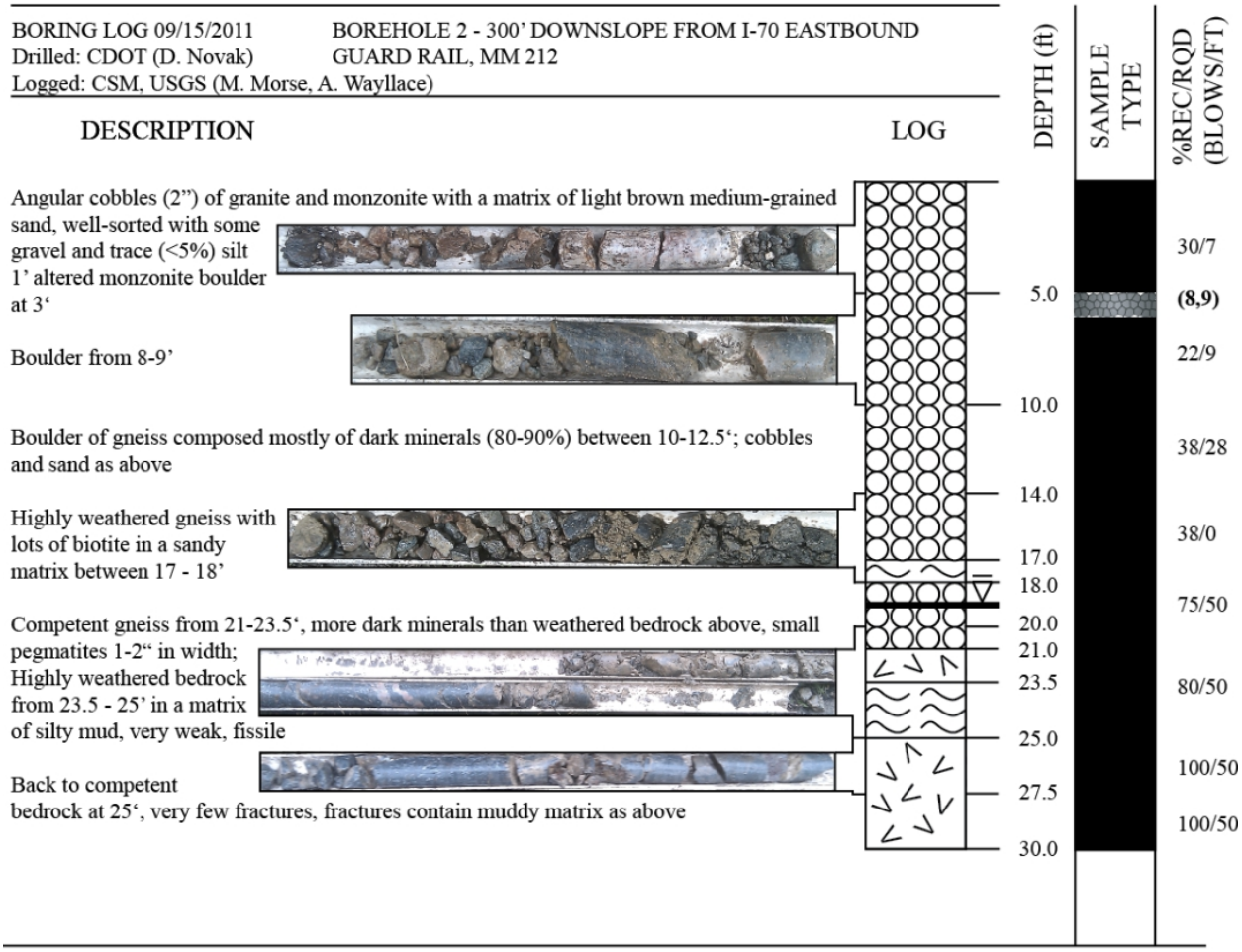

CALIFORNIA SAMPLE DESCRIPTION (5')

Liner 1: No recovery
Liner 2: No recovery
Liner 3: No recovery
Liner 4: **SW-SM** Brown silty sand with cm-scale gravel (10%)

DRILL NOTES

Drill rig: CME 55/300
Drill bit inner diameter = 2.5"
Total depth = 30.0'

LEGEND

Core sample
California sample
Cobbles with sandy or silty matrix
Highly weathered gneiss
More competent gneiss; bedrock

BORING LOG 08/03/2012
Drilled: CDOT (D. Novak)
Logged: CSM (M. Morse, A. Wayllace)

BOREHOLE 10 - EASTBOUND I-70 SHOULDER AT MM 212, ~50 FT WEST OF EASTERN EXTENT OF SLIDE

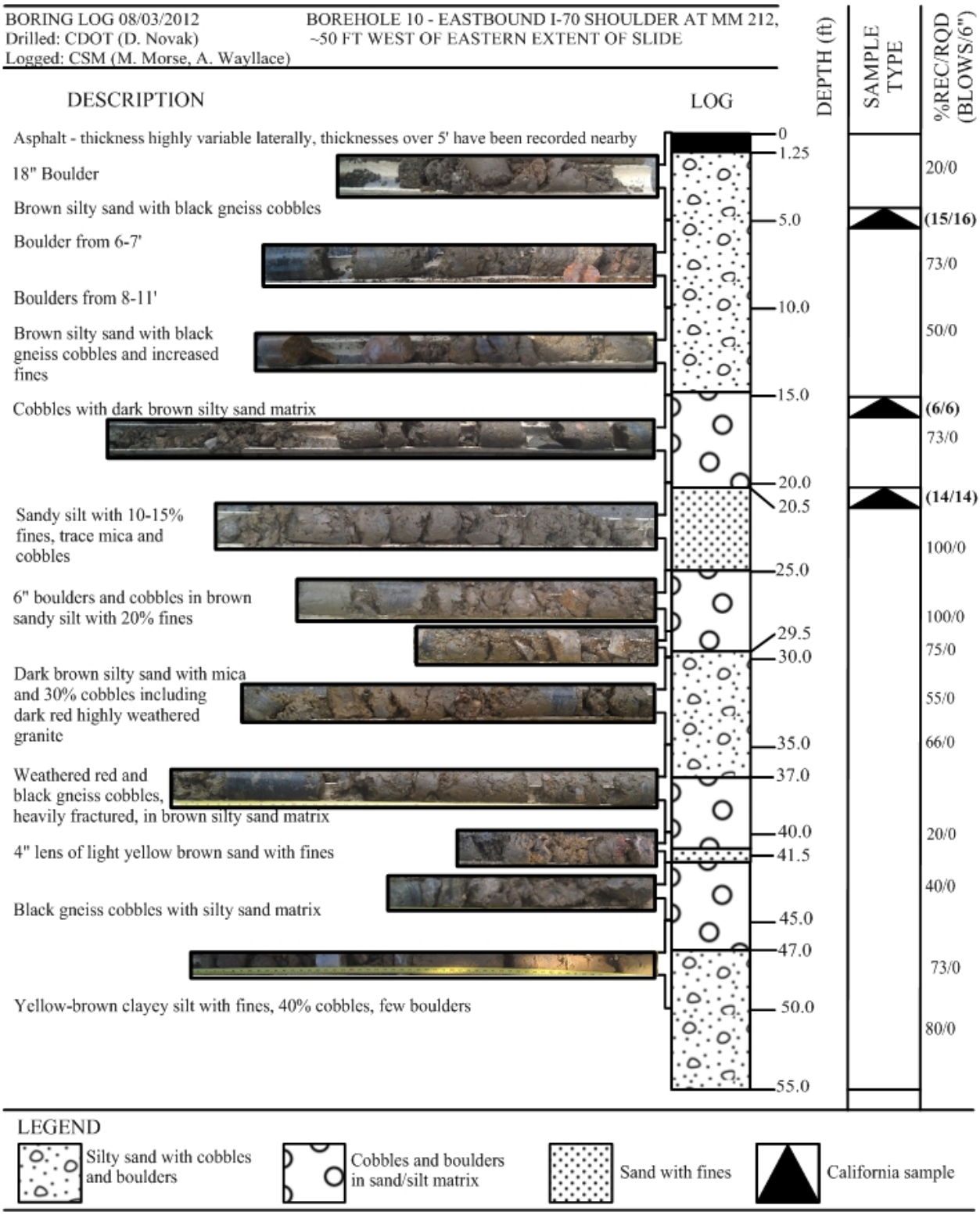

LEGEND

Silty sand with cobbles and boulders

Cobbles and boulders in sand/silt matrix

Sand with fines

California sample

BORING LOG 08/03/2012
Drilled: CDOT (D. Novak)
Logged: CSM (M. Morse, A. Wayllace)

BOREHOLE 10 - EASTBOUND I-70 SHOULDER AT MM 212, ~50 FT WEST OF EASTERN EXTENT OF SLIDE

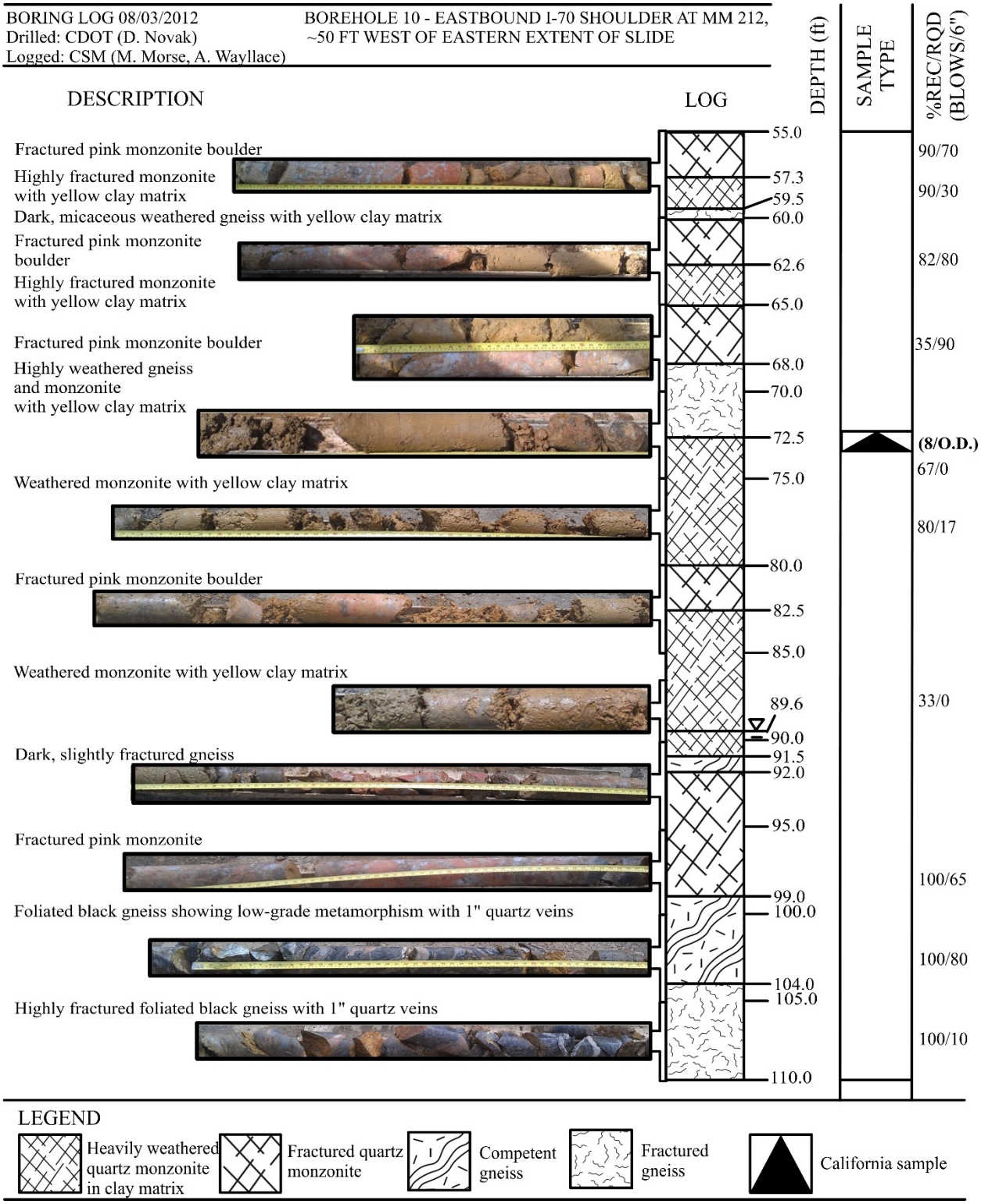

BORING LOG 11/10/2015
Drilled: CDOT (A. Moreno)
Logged: CDOT (J. Sieberg)

BOREHOLE 4 – 70M UPSLOPE OF I-70 SHOULDER, MM 212.0-212.1

Description	Depth	RQD
Colluvium top soil	3’	
Highly fractured granite and gneiss, pebble size pieces, clean fractures	20’	0% 18%
Less fractured granite with muscovite veins	33’	0% 48%
Heavily weathered granite with trace clay infilling	36’	0%
Off-white granite bedrock with some horizontal fractures and muscovite zones	40’	95%
	50’	

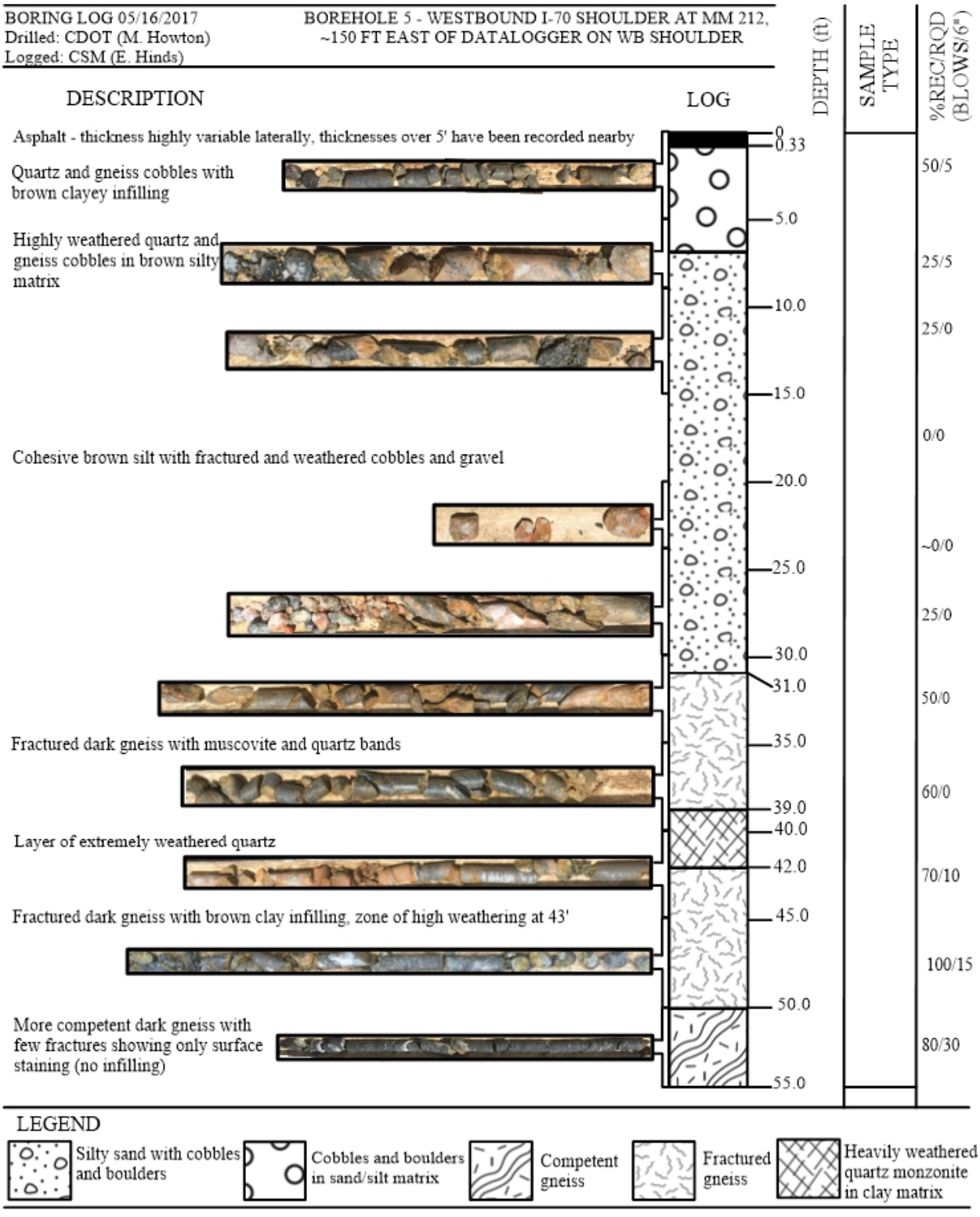
BORING LOG 05/16/2017
Drilled: CDOT (M. Howton)
Logged: CSM (E. Hinds)
BOREHOLE 5 - WESTBOUND I-70 SHOULDER AT MM 212, ~150 FT EAST OF DATALOGGER ON WB SHOULDER
DESCRIPTION
LOG
DEPTH (ft)
SAMPLE TYPE
%REC/RQD (BLOWS/6")
Asphalt - thickness highly variable laterally, thicknesses over 5' have been recorded nearby
Quartz and gneiss cobbles with brown clayey infilling
Highly weathered quartz and gneiss cobbles in brown silty matrix
Cohesive brown silt with fractured and weathered cobbles and gravel
Fractured dark gneiss with muscovite and quartz bands
Layer of extremely weathered quartz
Fractured dark gneiss with brown clay infilling, zone of high weathering at 43'
More competent dark gneiss with few fractures showing only surface staining (no infilling)
0
0.33
5.0
10.0
15.0
20.0
25.0
30.0
31.0
35.0
39.0
40.0
42.0
45.0
50.0
55.0
50/5
25/5
25/0
0/0
~0/0
25/0
50/0
60/0
70/10
100/15
80/30
LEGEND
Silty sand with cobbles and boulders
Cobbles and boulders in sand/silt matrix
Competent gneiss
Fractured gneiss
Heavily weathered quartz monzonite in clay matrix

BORING LOG 05/16/2017
Drilled: CDOT (M. Howton)
Logged: CSM (E. Hinds)

BOREHOLE 5 - WESTBOUND I-70 SHOULDER AT MM 212, ~150 FT EAST OF DATALOGGER ON WB SHOULDER

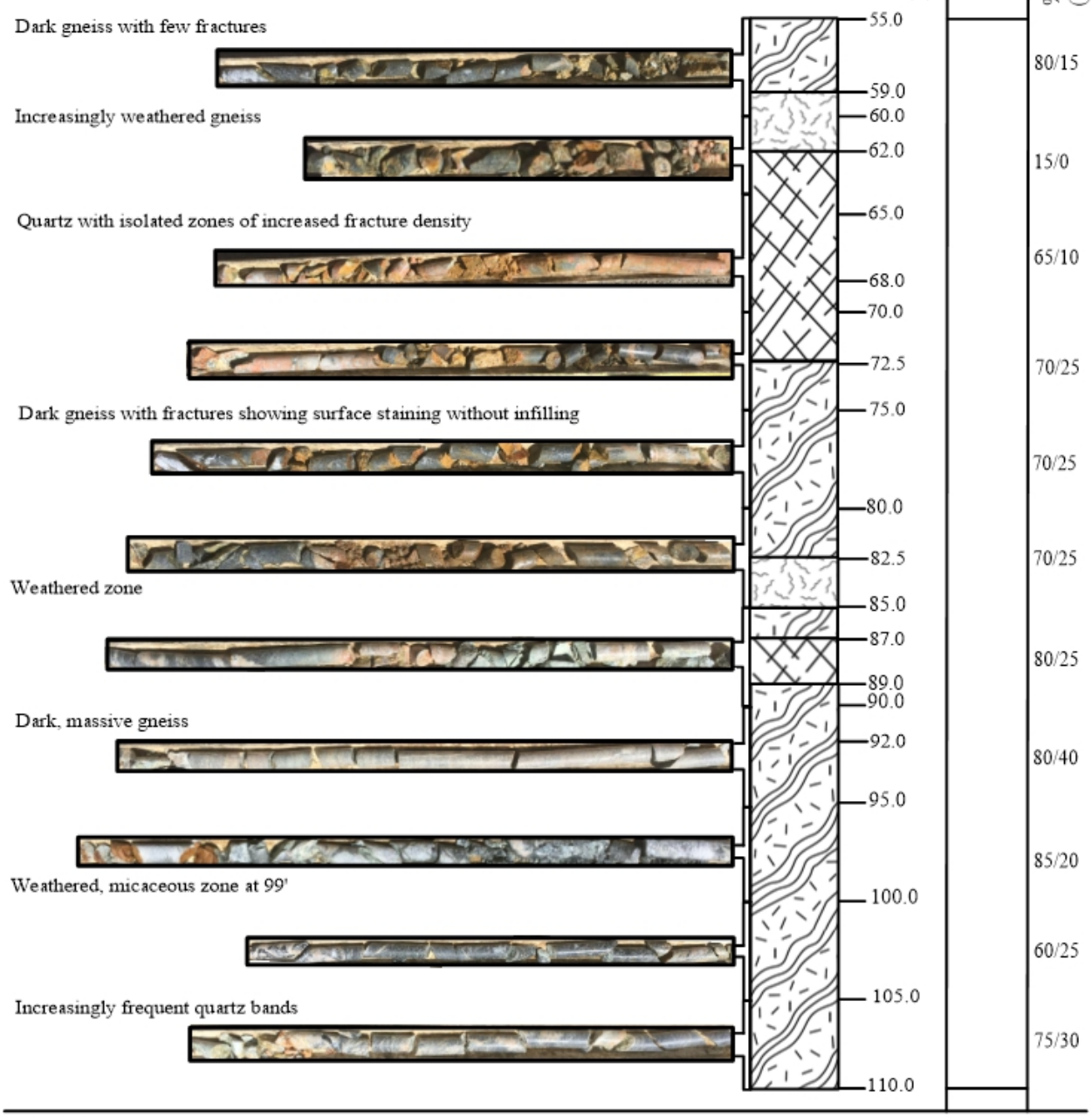

LEGEND

Fractured quartz monzonite

Competent gneiss

Fractured gneiss

BORING LOG 05/24/2017
Drilled: CDOT (M. Howton)
Logged: CSM (E. Hinds)

BOREHOLE 6 - WESTBOUND I-70 SHOULDER AT MM 212, ~450 FT WEST OF DATALOGGER ON WB SHOULDER

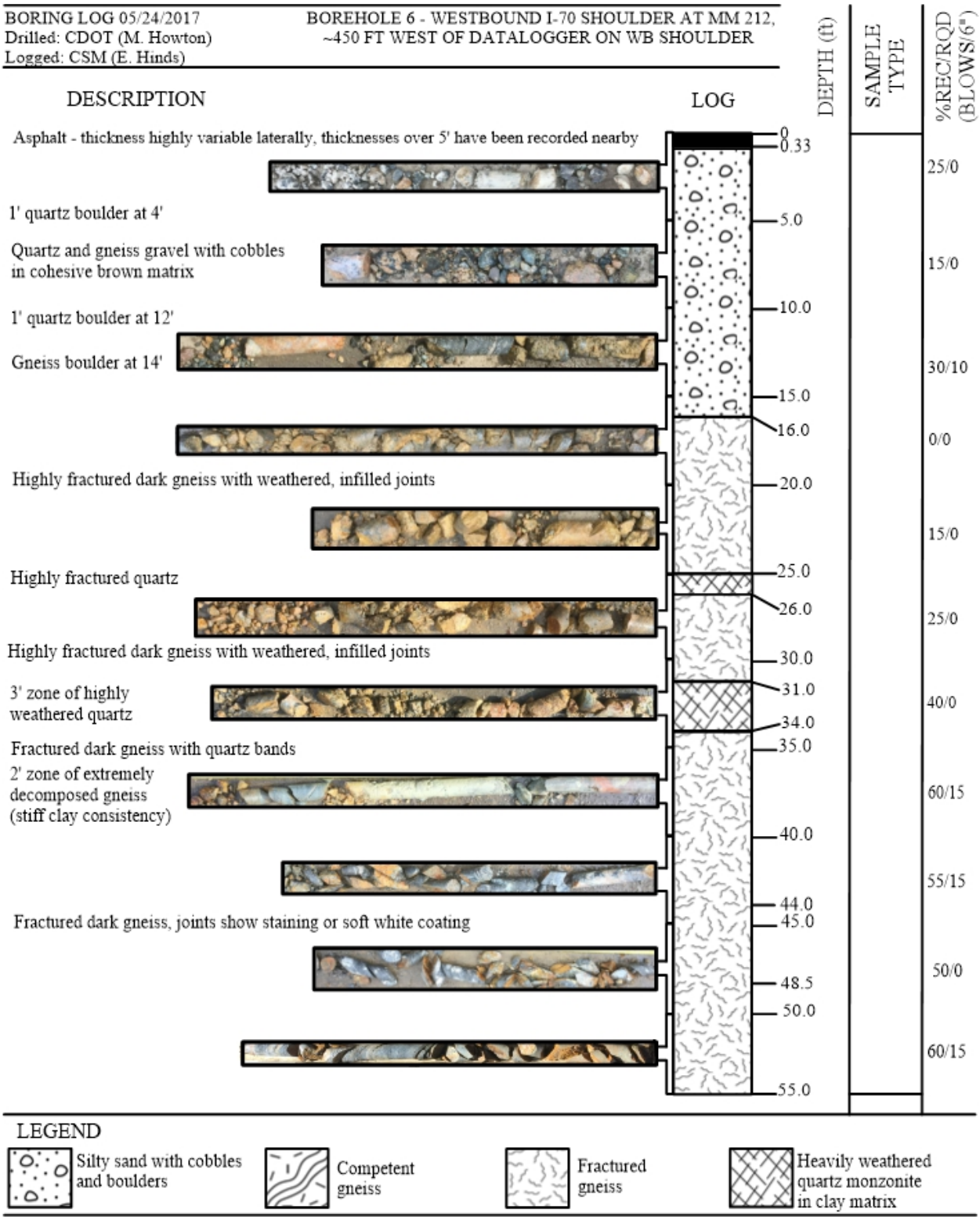

BORING LOG 05/24/2017
Drilled: CDOT (M. Howton)
Logged: CSM (E. Hinds)

BOREHOLE 6 - WESTBOUND I-70 SHOULDER AT MM 212, ~450 FT WEST OF DATALOGGER ON WB SHOULDER

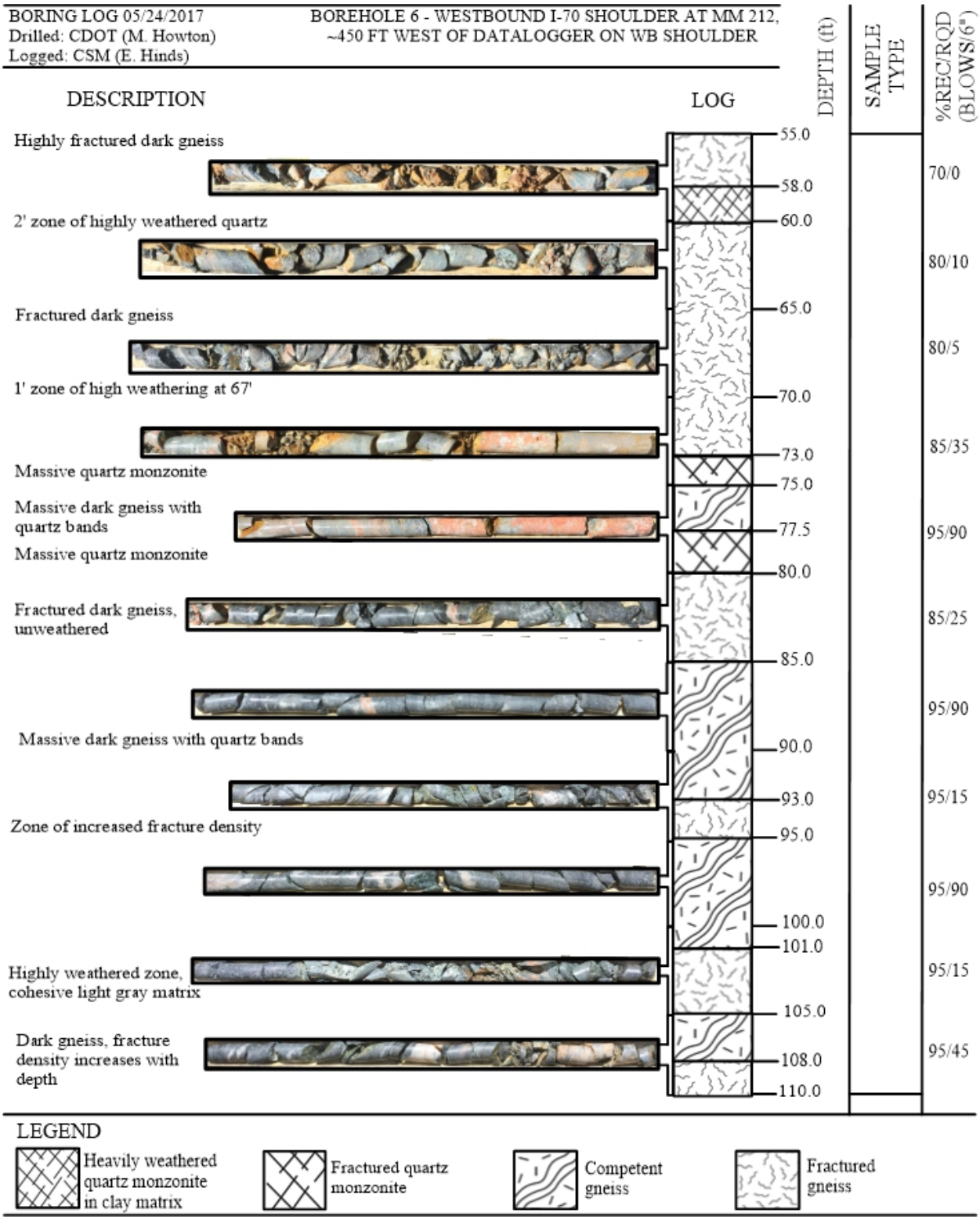

BORING LOG 07/18/2017
Drilled: CDOT (M. Howton)
Logged: CSM (E. Hinds)

BOREHOLE 7 - SLOPE NORTH OF I-70, ~165 FT EAST OF BOREHOLE 4

DESCRIPTION	DEPTH (ft)	SAMPLE TYPE	%REC/RQD (BLOWS/6")
Well weathered gravel and cobbles of mixed light gray to dark gray gneiss, gray and red granite, and red quartz in a brown, cohesive, silty matrix	0		50/15
	5.0		60/10
Red, white, and pink quartz boulders, ~8" thick	10.0		80/20
	15.0		70/20
	19.0		
Massive, mottled white and pink quartz with lightly stained fractures	20.0		100/90
Gravel-sized clasts observed along some fractures, no other significant infill	25.0		90/85
	30.0		
Gravel to coarse sand size quartz in very cohesive pale gray to brown clay matrix	32.0		80/60
Highly micaceous clasts from 39' to 41'	35.0		20/0
	40.0		
Mottled white and red quartz, fractures spaced ~3", fracture surfaces smooth and weathered	41.0		40/0
	45.0		
6" granitic intrusion at 49'			90/5
	50.0		
Red and white quartz with cohesive orange-brown infill	50.5		100/80
Red and white quartz with no infill, unweathered fracture faces	55.0		
	58.0		80/10
Dark, fine-grained gneiss from 58', steep fracture angles, thin non-cohesive light brown infill	60.0		

LOG

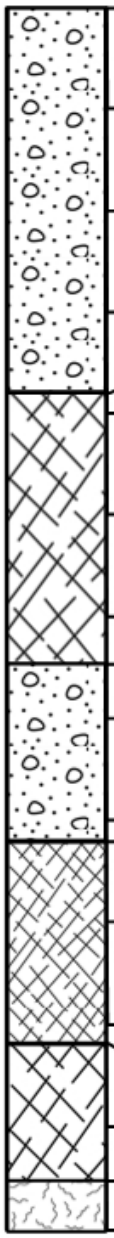

LEGEND


Cobbles and gravel in silty matrix


Heavily weathered quartz monzonite in clay matrix


Fractured quartz monzonite


Fractured gneiss

BORING LOG 07/20/2017
Drilled: CDOT (M. Howton)
Logged: CSM (E. Hinds)

BOREHOLE 8 - SLOPE NORTH OF I-70, ~430 FT WEST OF BOREHOLE 4

DESCRIPTION	DEPTH (ft)	SAMPLE TYPE	%REC/RQD (BLOWS/6")
Well weathered gravel and cobbles of mixed light gray to dark gray gneiss, gray and red granite, and red quartz in a brown, cohesive, silty matrix	0 – 5.0		5/0
Fractured dark gneiss with cohesive brown infill	5.0 – 7.5		50/20
Fractured white and pink quartz, dark pegmatism, cohesive brown infill	7.5 – 10.0		
Fractured dark gneiss with cohesive brown infill	10.0 – 10.5		65/45
Well weathered gravel and cobbles of mixed light gray to dark gray gneiss, gray and red granite, and red quartz in a brown, cohesive, silty matrix	10.5 – 15.0		10/0
8" thick dark gneiss boulder	15.0 – 20.0		15/0
Dark red quartz, fractures spaced at least 5", some coarse sand size clasts	20.0 – 23.5		
Mottled white and red quartz, increasingly micaceous, same fracture characteristics	23.5 – 25.0		100/90
Mottled white and red quartz, less micaceous, fractures show staining	25.0 – 30.0		100/90
	30.0 – 35.0		90/85
	35.0 – 40.0		80/60
	40.0 – 45.0		90/80
	45.0 – 50.0		100/80
	50.0 – 55.0		95/85
	55.0 – 60.0		

LOG

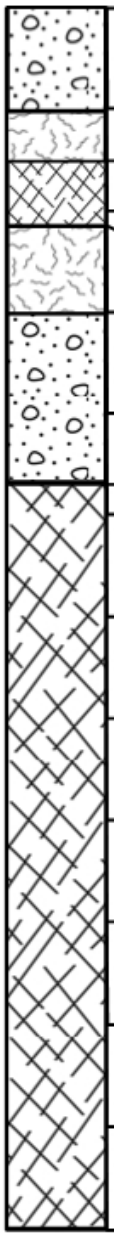

LEGEND


Cobbles and gravel in silty matrix


Heavily weathered quartz monzonite in clay matrix


Fractured quartz monzonite


Fractured gneiss

APPENDIX B
FIELD INSTRUMENTATION

Equipment: 2 Campbell Scientific CR10X dataloggers
2 Campbell Scientific AVW200 vibrating wire analyzers
1 Campbell Scientific AM16/32B multiplexer
8 Geokon 4500S vibrating wire piezometers

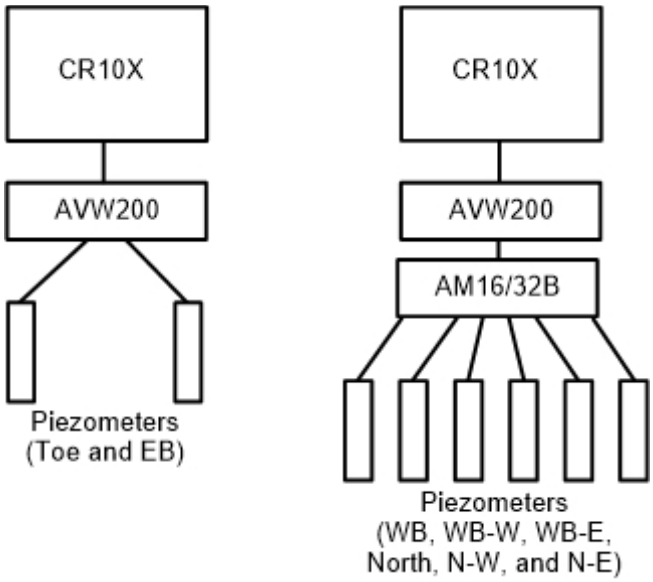

Figure B.1. Datalogger setup; eastbound (left) and westbound (right).

Software: PC200W (datalogger communication)
Loggernet (datalogger programming)

Installation:

1) Piezometers were calibrated in laboratory by saturating filter tip, taking readings at known atmospheric pressure and temperature, and back-calculating polynomials per the Geokon 4500S manual (Geokon, 2018) and Thunder (2016).

The pressure calculation used for calibration is given by:

$$P = AD^2 + BD + C + K(T_i - T_0) \quad \text{(B.1)}$$

where *A, B,* and *K* are factory-supplied coefficients; *C* is back-calculated from the zero reading taken during laboratory calibration; and *D* is the piezometer reading in digits:

$$D = \frac{Hz^2}{1000} \quad \text{(B.2)}$$

where T_0 is the temperature in °C during zero reading, and T_i is the current temperature in °C calculated from piezometer thermistor resistance, *R*, as

$$T_i = \frac{1}{(1.4051*10^{-3})+(2.369*10^{-4})ln\,R+(1.1019*10^{-7})(ln\,R)^3} - 273.2 \quad \text{(B.3)}$$

or each piezometer are given in Table B.1.

Table B.1 Piezometer Calibration Factors

Piezometer	A [kPa·digit^{-2}]	B [kPa·digit^{-1}]	K [kPa/°C]	Temperature at Zero Reading [°C]	Zero Reading [digits]	C [kPa]
WB	1.38E-07	-0.0963	0.0443	16.1	9277.5	881.545
Toe	-8.73E-08	-0.1049	0.0853	3.7	9231.7	975.845
EB	8.61E-08	-0.0969	-0.0755	7.9	9370.2	900.414
North	-3.34E-07	-0.106	-0.04498	4.6	9124.1	994.960
WB-East	-2.50E-07	-0.1069	0.01486	21.7	8895.9	970.764
WB-West	-2.83E-07	-0.0985	0.07024	20.6	8944.3	903.181
North-East	-2.51E-07	-0.1153	0.01486	20.6	9255.6	1088.629
North-West	-1.04E-07	-0.1147	-0.04159	21.0	9156.7	1058.982

2) Following completion of each 50-foot borehole drilling, a 1.5" diameter PVC pipe casing was installed to the bottom of the borehole, with its lowest 20 ft screened and all else solid.

3) Field calibration was performed by taking a reading at an arbitrary depth below the groundwater table, lowering the piezometer by a known distance, and checking the calculated pressure head difference. Piezometers were installed with tips facing upwards to prevent air bubble entrapment.

4) Inside and outside of each PVC casing, the boreholes were backfilled with clean sand for 20 ft, bentonite for 10 ft above that, clean sand to approximately 10 ft from the ground surface, and a final bentonite cap for the remaining 10 ft. This backfilling was intended to allow full hydraulic connectivity between the piezometer and surrounding groundwater, without causing the borehole to act as a preferential flow path and increase recorded pressure heads.

5) Piezometer cables were spliced as necessary and run through flexible aluminum conduit for protection from animals, falling branches, movement of surficial materials, and other disruptions.

APPENDIX C
List of *.csv data files

Data files for field measurements (See Figure C.1):

1. EB.csv (field data East Bound piezometer)
2. North.csv (field data North piezometer)
3. NorthEast.csv (field data North East piezometer)
4. NorthWest.csv (field data North West piezometer)
5. Toe.csv (field data Toe piezometer)
6. WB.csv (field data West Bound piezometer)
7. WBEast.csv (field data West Bound East piezometer)
8. WBWest.csv (field data West Bound West piezometer)

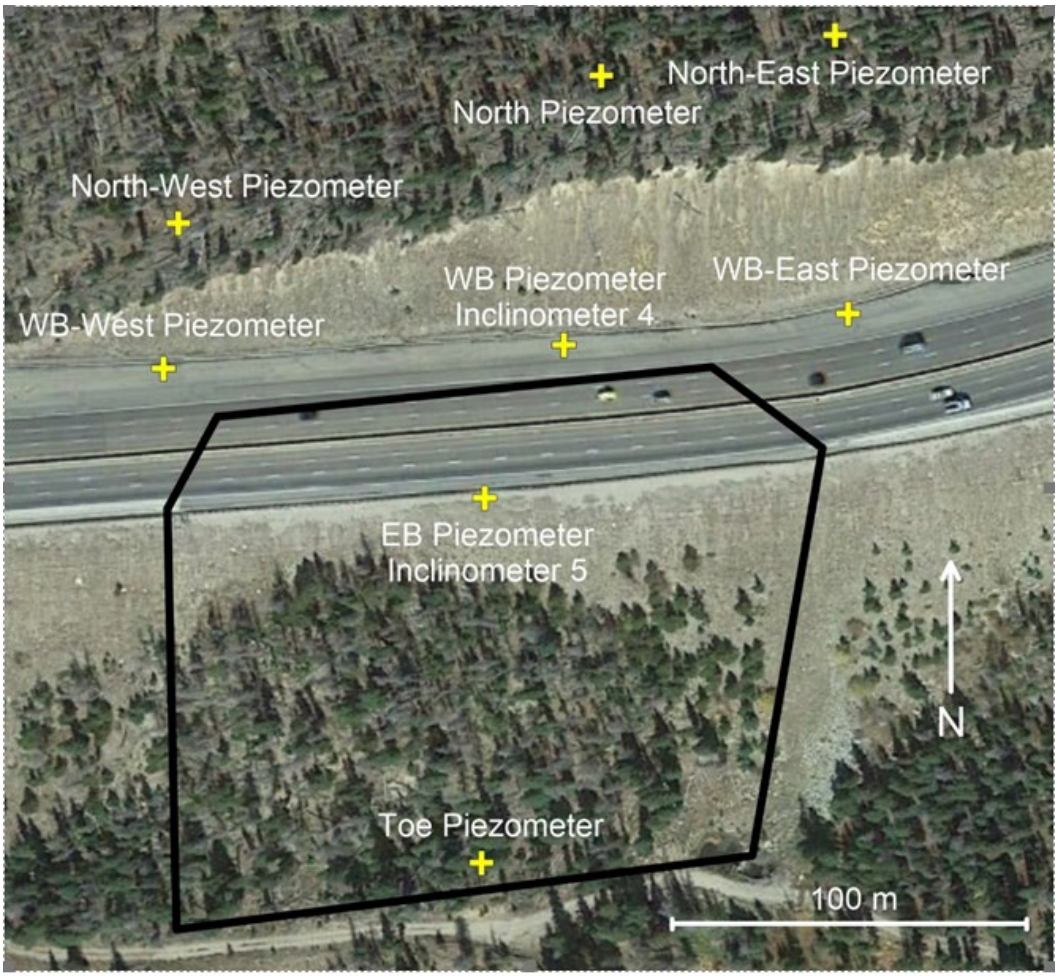

Figure C.1. Piezometer locations with approximate slide extents shown in black (from Hinds, 2018).

Data file for numerical modeling:

9. Modeled_obs_points.csv (file with data from observation points that match West Bound piezometer, East Bound piezometer, and Toe piezometer.)